NUREG/IA-0551

International Agreement Report

Assessment of 3D Components in System Codes Against Separate Effect Tests

Prepared by:
Yunseok Lee*, Taewan Kim*, Jae Soon Kim**, Dong Gu Kang**

*Department of Safety Engineering,
Incheon National University,
119 Academy-ro, Yeonsu-gu,
Incheon 22012, Republic of Korea

**Korea Institute of Nuclear Safety (KINS)
62 Gwahak-ro, Yuseong-gu,
Daejeon 34142, Republic of Korea

A. Hsieh, NRC Project Manager

Division of Systems Analysis
Office of Nuclear Regulatory Research
U.S. Nuclear Regulatory Commission
Washington, DC 20555-0001

Manuscript Completed: August 2024
Date Published: June 2025

Prepared as part of
The Agreement on Research Participation and Technical Exchange
Under the Thermal-Hydraulic Code Applications and Maintenance Program (CAMP)

Published by
U.S. Nuclear Regulatory Commission

AVAILABILITY OF REFERENCE MATERIALS IN NRC PUBLICATIONS

NRC Reference Material

As of November 1999, you may electronically access NUREG-series publications and other NRC records at NRC's Library at www.nrc.gov/reading-rm.html. Publicly released records include, to name a few, NUREG-series publications; *Federal Register* notices; applicant, licensee, and vendor documents and correspondence; NRC correspondence and internal memoranda; bulletins and information notices; inspection and investigative reports; licensee event reports; and Commission papers and their attachments.

NRC publications in the NUREG series, NRC regulations, and Title 10, "Energy," in the *Code of Federal Regulations* may also be purchased from one of these two sources.

1. **The Superintendent of Documents**
   U.S. Government Publishing Office
   Washington, DC 20402-0001
   Internet: https://bookstore.gpo.gov/
   Telephone: (202) 512-1800
   Fax: (202) 512-2104

2. **The National Technical Information Service**
   5301 Shawnee Road
   Alexandria, VA 22312-0002
   Internet: https://www.ntis.gov/
   1-800-553-6847 or, locally, (703) 605-6000

A single copy of each NRC draft report for comment is available free, to the extent of supply, upon written request as follows:

Address: **U.S. Nuclear Regulatory Commission**
Office of Administration
Digital Communications and Administrative Services Branch
Washington, DC 20555-0001
E-mail: Reproduction.Resource@nrc.gov
Facsimile: (301) 415-2289

Some publications in the NUREG series that are posted at NRC's Web site address www.nrc.gov/reading-rm/doc-collections/nuregs are updated periodically and may differ from the last printed version. Although references to material found on a Web site bear the date the material was accessed, the material available on the date cited may subsequently be removed from the site.

Non-NRC Reference Material

Documents available from public and special technical libraries include all open literature items, such as books, journal articles, transactions, *Federal Register* notices, Federal and State legislation, and congressional reports. Such documents as theses, dissertations, foreign reports and translations, and non-NRC conference proceedings may be purchased from their sponsoring organization.

Copies of industry codes and standards used in a substantive manner in the NRC regulatory process are maintained at—

The NRC Technical Library
Two White Flint North
11545 Rockville Pike
Rockville, MD 20852-2738

These standards are available in the library for reference use by the public. Codes and standards are usually copyrighted and may be purchased from the originating organization or, if they are American National Standards, from—

American National Standards Institute
11 West 42nd Street
New York, NY 10036-8002
Internet: www.ansi.org
(212) 642-4900

Legally binding regulatory requirements are stated only in laws; NRC regulations; licenses, including technical specifications; or orders, not in NUREG-series publications. The views expressed in contractor prepared publications in this series are not necessarily those of the NRC.

The NUREG series comprises (1) technical and adminis-trative reports and books prepared by the staff (NUREG–XXXX) or agency contractors (NUREG/CR–XXXX), (2) proceedings of conferences (NUREG/CP–XXXX), (3) reports resulting from international agreements (NUREG/IA–XXXX),(4) brochures (NUREG/BR–XXXX), and (5) compilations of legal decisions and orders of the Commission and Atomic and Safety Licensing Boards and of Directors' decisions under Section 2.206 of NRC's regulations (NUREG–0750),and (6) Knowledge Management prepared by NRC staff or agency contractors.

NUREG/IA-0551

International Agreement Report

Assessments of 3D Components in System Codes Against Separate Effect Tests

Prepared by:
Yunseok Lee*, Taewan Kim*, Jae Soon Kim**, Dong Gu Kang**

*Department of Safety Engineering,
Incheon National University,
119 Academy-ro, Yeonsu-gu,
Incheon 22012, Republic of Korea

**Korea Institute of Nuclear Safety (KINS)
62 Gwahak-ro, Yuseong-gu,
Daejeon 34142, Republic of Korea

A. Hsieh, NRC Project Manager

Division of Systems Analysis
Office of Nuclear Regulatory Research
U.S. Nuclear Regulatory Commission
Washington, DC 20555-0001

Manuscript Completed: August 2024
Date Published: June 2025

Prepared as part of
The Agreement on Research Participation and Technical Exchange
Under the Thermal-Hydraulic Code Applications and Maintenance Program (CAMP)

Published by
U.S. Nuclear Regulatory Commission

ABSTRACT

As research focus intensifies on employing multi-rod representation for loss-of-coolant accidents (LOCA) analysis, the use of three-dimensional (3D) components of system codes has become essential for modeling the subchannel-scale multi-rod scheme. However, utilizing system codes at this subchannel-scale level is a novel endeavor, necessitating a comprehensive assessment of their capability. This study assesses the 3D components within the TRACE V5 patch 7 and MARS-KS 2.0 system codes against two separate effect tests: GE 3X3 and PSBT bundle experiments. The assessment confirmed that the 3D components of both codes inadequately predicted the phasic distribution observed in the experiments. Notably, TRACE significantly overpredicted vapor in comparison to MARS-KS. The discrepancy in vapor estimation between TRACE and MARS-KS stemmed from differing approaches to interfacial drag calculations. TRACE's application of a drift flux model for vertical and horizontal flows led to larger interfacial drag calculations, resulting in underestimation of crossflows. In contrast, MARS-KS employed a drag coefficient model for horizontal flow, yielding smaller interfacial drag and increased crossflows, dispersing vapor throughout the entire cross-section of the bundle. These findings underscored the critical role of crossflow in subchannel-scale analysis, highlighting the imperative need to enhance crossflow models in both codes for accurate prediction of phasic distribution in the bundle. As a proposed improvement, this study suggests adopting the subchannel-mixing model—a turbulence model commonly used in state-of-the-art subchannel analysis codes. Notably, enhancing crossflows significantly bolstered the general code predictability, particularly when implementing secondary transport of two-phase mixtures using the subchannel mixing model.

FOREWORD

The Korea Institute of Nuclear Safety (KINS) prepared this report under the Implementing Agreement on Thermal-Hydraulic Code Applications and Maintenance Program between the United States Nuclear Regulatory Commission (USNRC) and KINS (signed in 2023).

KINS presented the results of this study at the 2023 Fall CAMP meeting and proposed it as an in-kind contribution during the Technical Program Committee (TPC) meeting.

TABLE OF CONTENTS

LIST OF FIGURES

LIST OF TABLES

EXECUTIVE SUMMARY

This study aims to assess the 3D components in the system codes, TRACE V5.0 patch 7 and MARS-KS 2.0, focusing on multi-rod simulation. It compares their performance against two widely used Separate Effect Tests (SETs): GE 3X3 and PSBT bundle experiments, commonly employed for subchannel analysis code validation. By comparing the calculated results of both 3D models of system codes against experimental data, the study evaluates their predictability at the subchannel-scale level.

The assessment revealed that both codes inadequately predicted the phasic distribution of the experiments. Moreover, TRACE significantly overestimated vapor compared to MARS-KS due to its extensive calculation of interfacial drag on crossflows. This excessive calculation reduced net mixing between channels, confining vapor within individual subchannels in the bundle.

TRACE tended to overcalculate interfacial drag for crossflows by employing the drift flux model. In contrast, MARS-KS calculated relatively smaller interfacial drag compared to TRACE, utilizing the drag coefficient model for crossflow calculations.

The code predictions exhibited significant sensitivity to interfacial drag calculations. Notably, when MARS-KS adopted TRACE's model with large interfacial drag in crossflow calculations, it also led to an overprediction of void fraction. This highlighted the substantial importance of crossflow calculations in subchannel-scale analysis.

The inadequate code predictions of phasic distribution of the experiments were attributed to insufficient crossflow calculations necessary at the subchannel-scale level. The presence of the rod bundle caused substantial flow perturbations, resulting in significant secondary flows between channels. These secondary flows induced shifts in both vapor and liquid phases, thereby affecting the phasic distribution within the bundle.

Most state-of-the-art subchannel analysis codes incorporate the subchannel mixing model to account for these secondary flow effects. This study confirmed its effectiveness by integrating the subchannel mixing model into MARS-KS and comparing the outcomes with the original calculations. The results notably demonstrated improved code predictions, underscoring the importance of enhancing crossflow for subchannel-scale analysis using these system codes.

Therefore, as an improvement proposal, this study suggests improving the crossflow models of both system codes by integrating the subchannel mixing model to facilitate multi-rod analysis within both systems.

NOMENCLAUTRE

α_g	Void fraction, Vapor volume fraction $[-]$
α_d	Droplet volume fraction $[-]$
α_{flim}	Volume fraction of annular film $[-]$
ρ_g	Vapor density $[kg/m^3]$
ρ_f	Liquid density $[kg/m^3]$
μ_f	Liquid viscosity $[kg/m \cdot s]$
σ	Surface tension $[N/m]$
A_i'''	Interfacial area per unit volume $[1/m]$
A_{jun}	Junction area $[m^2]$
A_{vol}	Volume-averaged area $[m^2]$
C_i	Interfacial friction coefficient $[N \cdot s^2/m^5]$
C_d	Drop drag coefficient $[-]$
D_h	Hydraulic diameter $[m]$
d_d	Droplet diameter $[m]$
Re_d	Drop Reynolds number $[-]$
v_{gj}	Drift velocity $[m/s]$

1 INTRODUCTION

The significance of thermal-hydraulic (TH) system codes lies in evaluating the system performance of nuclear power plants during postulated accident conditions for design and regulatory purposes. Thus, conservatism was the primary concern in system code analysis [1]. However, the perspective shifted as best-estimate analyses for large-break loss-of-coolant accidents (LBLOCA) has been allowed. This change broadened the scope of system code analysis to enable realistic predictions of reactor transients and accidents as much as possible [2].

System codes utilized for best-estimate analyses are referred to as best-estimate system codes. State-of-the-art best-estimate system codes are predominantly equipped with three-dimensional (3D) components. The significance of these 3D components lies in their ability to analyze multi-dimensional phenomena, a challenge when using conventional one-dimensional (1D) components [3].

Recently, regulatory focus has zeroed in on multi-rod behavior due to the potential risks associated with high burnup fuels and the potential core damage due to extreme fuel rod deformation during accidents, as depicted in Figure 1-1 [4]. This concern not only prompted consideration of corresponding phenomena within the reactor core but also necessitated a multi-rod representation. Consequently, the use of 3D components in the system codes has been expanded to model the reactor core based on the subchannel-scale multi-rod representation.

However, using system codes at the subchannel-scale level was unprecedented, demanding an initial confirmation of the 3D components' sufficient capability within these system codes. Therefore, this study aimed to assess the 3D components in the best-estimate system codes, TRACE V5.0 patch 7 [6] and MARS-KS 2.0 [7], for the aforementioned subchannel-scale analysis. To achieve this, two separate effect tests (SETs), namely GE 3X3 [8] and PSBT [9], were employed for the assessment. The evaluation involved a code-to-code comparison to gauge the predictability of the 3D components in both system codes against experimental data and, subsequently, to compare their performance at the subchannel-scale level.

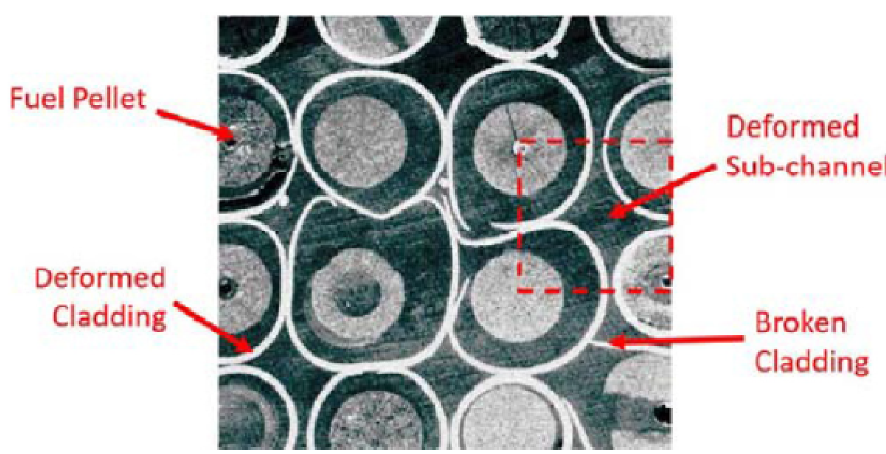

Figure 1-1 Rod Bundle Cross-Section After PHEBUS LOCA Experiment [Ref. 5]

2 DESCRIPTION OF ASSESSMENT MODELS

2.1 GE 3X3

The GE 3X3 test serves as one of the SETs utilized for validating subchannel analysis codes. It involved using water as the working fluid to measure mixture conditions within a rod bundle geometry [8].

Figure 2-1 depicts a schematic diagram of the test facility, designed to mimic a boiling water reactor (BWR) loop. The loop conditions were simulated using electrical heating from a nine-rod bundle within the test rig, maintaining a system pressure of 1000 psia (6.8947 MPa). As subcooled water passed through the test section, it received electrical heating from the rods, leading to boiling within the test section. Consequently, the coolant exited the test section as a two-phase mixture of water and vapor.

The specification of the test section is listed in Table 2-1. The test section consists of 16 subchannels having 72-inch (1.8288m) heated length. The nine rods featured uniform power distribution and consistent linear heat generation along the heated length. Measurements of mass flow rate and enthalpy of the steam-water mixture were taken at the exit of individual subchannels within the test section: corner, side, and center. These measurements were conducted under isokinetic conditions to minimize flow redistribution near the exit of test section.

The 3D components of both system codes were utilized to model the entire subchannels of the test section, detailed in Table 2-2. For the code-to-code comparison, the assessment models were configured with an identical modeling scheme. The heated section was represented using 36 uniform axial nodes, each with a node size of 2 inches (0.0508 m). Flow conditions were established by interconnecting dummy hydraulic volumes at the bottom of the heated section. To ensure equalized exit pressure within the test section, multiple pressure boundary volumes were connected to the exit of subchannels. In the case of TRACE, due to the restriction on direct connection between VESSEL and BREAK components, intermediate pipe volumes with the same node size were introduced between the pressure boundary and heated section volumes.

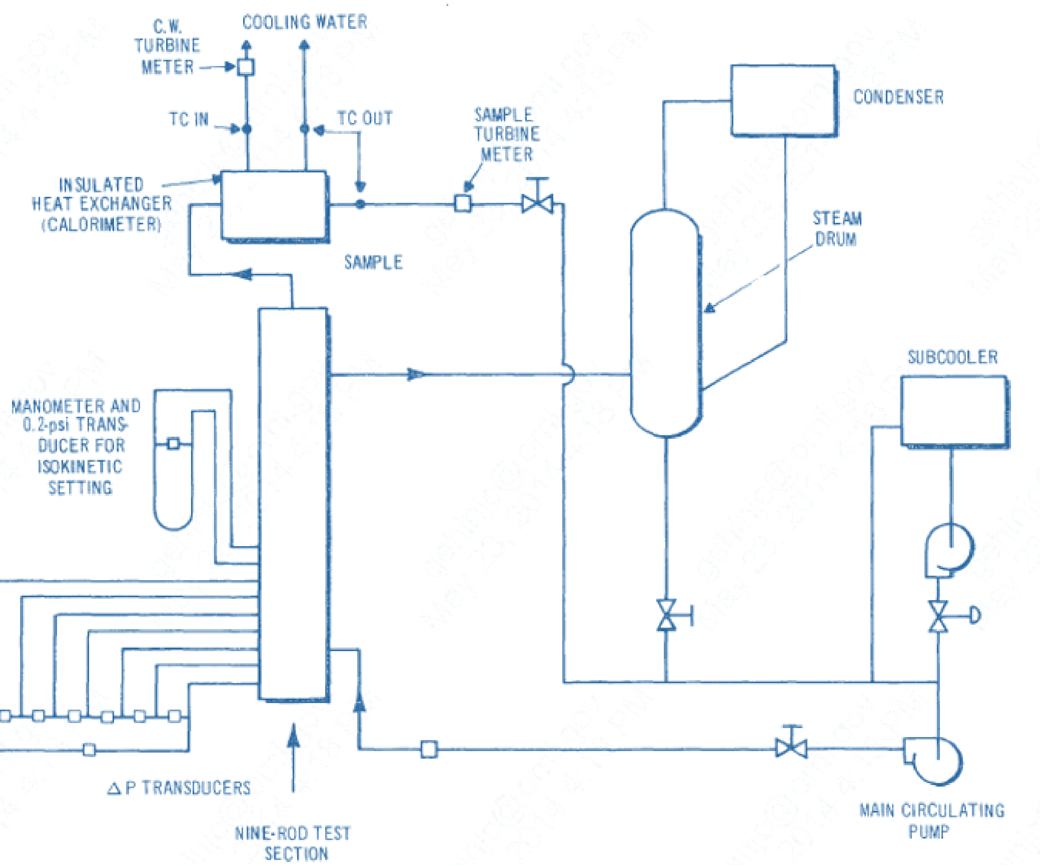

Figure 2-1 Schematic Diagram of GE 3X3 Test Facility [Ref. 8]

Table 2-1 Specification of GE 3X3 Test Section [Ref. 8]

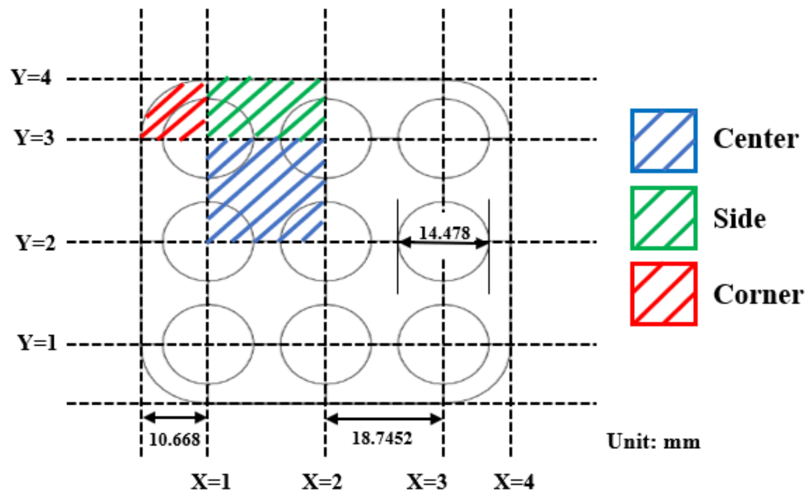

Cross-sectional view of test section

Parameter (unit)	Corner	Side	Center
Flow area (m^2)	5.049651×10^{-5}	1.176592×10^{-4}	1.867533×10^{-4}
Wetted perimeter (m)	2.834629×10^{-2}	4.148719×10^{-2}	4.548398×10^{-2}
Hydraulic diameter (m)	7.125661×10^{-3}	1.134414×10^{-2}	1.642365×10^{-2}
Heated length (m)	1.8288		
No. of spacers	6		
Spacer location (m)	0.0508, 0.3556, 0.6604, 0.9652, 1.270, 1.5748		

Table 2-2 Specification of the Assessment Models for GE 3X3 Test

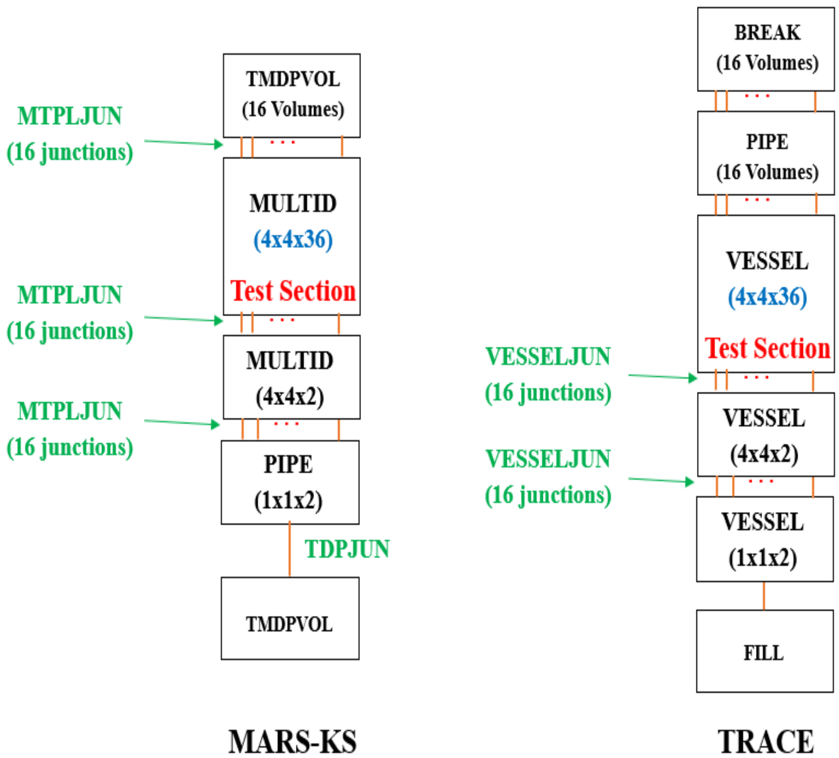

Parameter (unit)		Corner	Side	Center
Node volume (m^3)		5.7814×10^{-6}	1.0159×10^{-5}	1.7850×10^{-5}
Volume fraction (porosity)		4.4371×10^{-1}	5.8837×10^{-1}	5.3148×10^{-1}
Gap area per node (m^2)	Facing Corner	1.7419×10^{-4}	1.7419×10^{-4}	2.1677×10^{-4}
	Facing Center		2.1677×10^{-4}	
K-factor of spacer grid		0.336	0.1629	0.1504

2.2 PSBT Bundle

The PWR Subchannel and Bundle Test (PSBT) experiment focuses on void fraction measurement under PWR-type subchannel and bundle geometries. The database of the experiment covered wide range of two-phase flow conditions using water as the working fluid, including operation conditions in commercial pressurized water reactors. Consequently, this experiment serves as a widely used benchmark for validating subchannel analysis codes [9].

Figure 2-2 illustrates a schematic diagram of the bundle test facility, comprising 25 heater rods. Loop conditions were established by injecting subcooled water into the test rig and applying electrical heating to induce boiling within the test section. Void fraction measurements were taken across four central subchannels at different locations along the heated section: lower (2.216 m), middle (2.669 m), and upper (3.177 m).

Table 2-3 outlines the specifications of the test section, comprising 36 subchannels with a heated length of 144 inches (3.658 m). Notably, the power distribution of the equipped rods differs, with the centrally located nine rods having a higher power concentration compared to the peripheral rods. The test cases, namely B5 and B6, differ in axial power conditions: the B5 test features uniform axial power, while the B6 test applies a cosine-shaped axial power distribution.

The 3D components of both system codes were utilized to model the entire subchannels of the test section, as detailed in Table 2-4. For the code-to-code comparison, the assessment models were designed to maintain an identical modeling scheme. The heated section was represented by 72 axial nodes, each with an approximate 2-inch (0.0508 m) node size, depending on the location of spacer grids. In this setup, the form loss coefficients of spacer grids were uniformly applied across the cross-section of bundle. To establish flow conditions, dummy hydraulic volumes were interconnected at the bottom of the heated section, while multiple pressure boundary volumes were linked to the exit of subchannels to equalize the exit pressure of the test section.

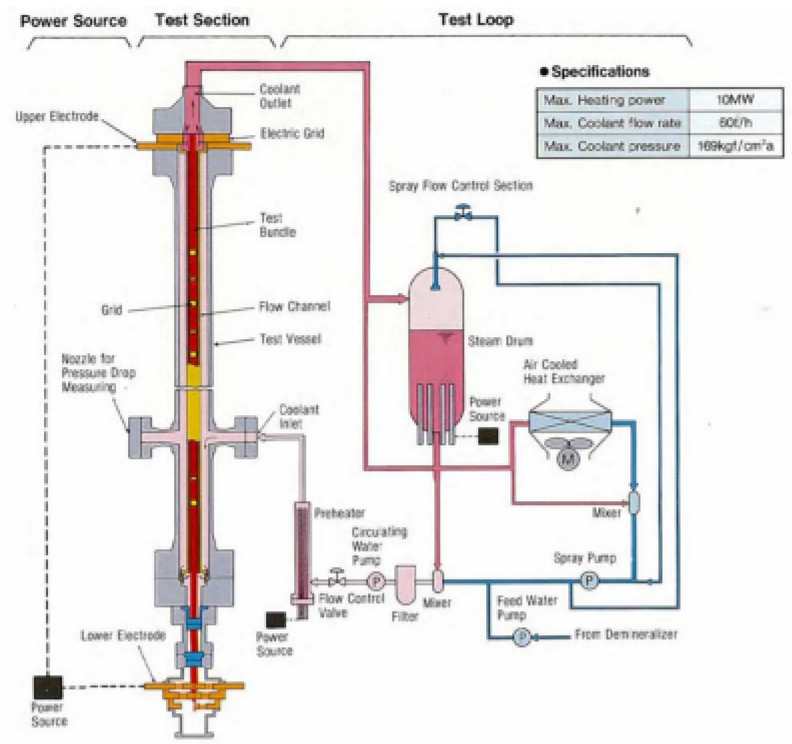

(a) Test loop

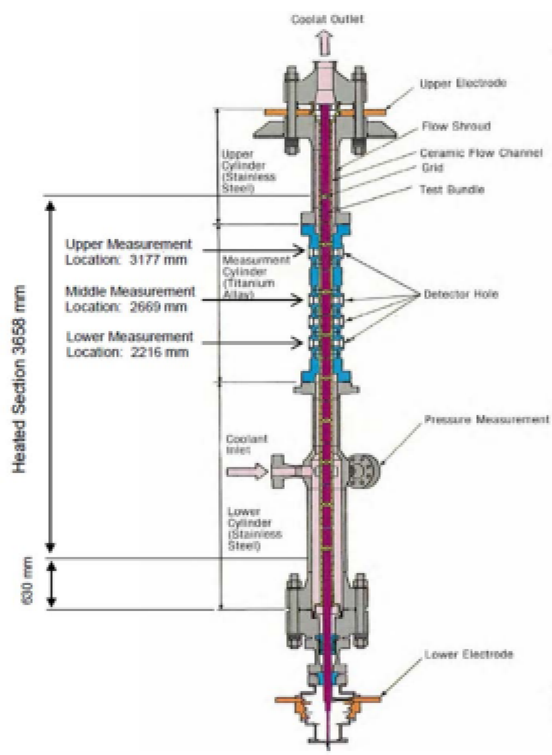

(b) Bundle Test section

Figure 2-2 Schematic Diagram of PSBT Bundle Test Facility [Ref. 9]

Table 2-3 Specification of PSBT Bundle Test Section [Ref. 9]

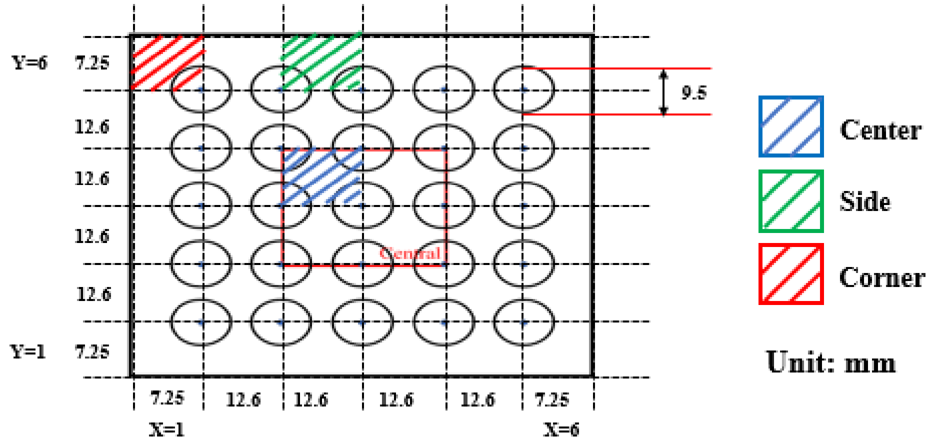

Cross-sectional view of test section (B5 & B6)

<table>
<tr><th colspan="2">Parameter (unit)</th><th>Corner</th><th>Side</th><th>Center</th></tr>
<tr><td colspan="2">Flow area (m^2)</td><td>3.484195×10^{-5}</td><td>5.590891×10^{-5}</td><td>8.787782×10^{-5}</td></tr>
<tr><td colspan="2">Wetted perimeter (m)</td><td>2.196128×10^{-2}</td><td>2.752257×10^{-2}</td><td>2.984513×10^{-2}</td></tr>
<tr><td colspan="2">Hydraulic diameter (m)</td><td>6.346069×10^{-3}</td><td>8.125537×10^{-2}</td><td>1.177784×10^{-2}</td></tr>
<tr><td colspan="2">Heated length (m)</td><td colspan="3">3.658</td></tr>
<tr><td rowspan="3">No. of spacers</td><td>Simple</td><td colspan="3">8</td></tr>
<tr><td>Mixing vane</td><td colspan="3">7</td></tr>
<tr><td>Non-mixing vane</td><td colspan="3">2</td></tr>
<tr><td rowspan="3">Spacer location (m)</td><td>Simple</td><td colspan="3">0.237, 0.698, 1.151, 1.605, 2.059, 2.512, 2.993, 3.501</td></tr>
<tr><td>Mixing vane</td><td colspan="3">0.471, 0.925, 1.378, 1.832, 2.285, 2.739, 3.247</td></tr>
<tr><td>Non-mixing vane</td><td colspan="3">0.0025, 3.755</td></tr>
</table>

Table 2-4 Specification of Assessment Models For PSBT Bundle Test

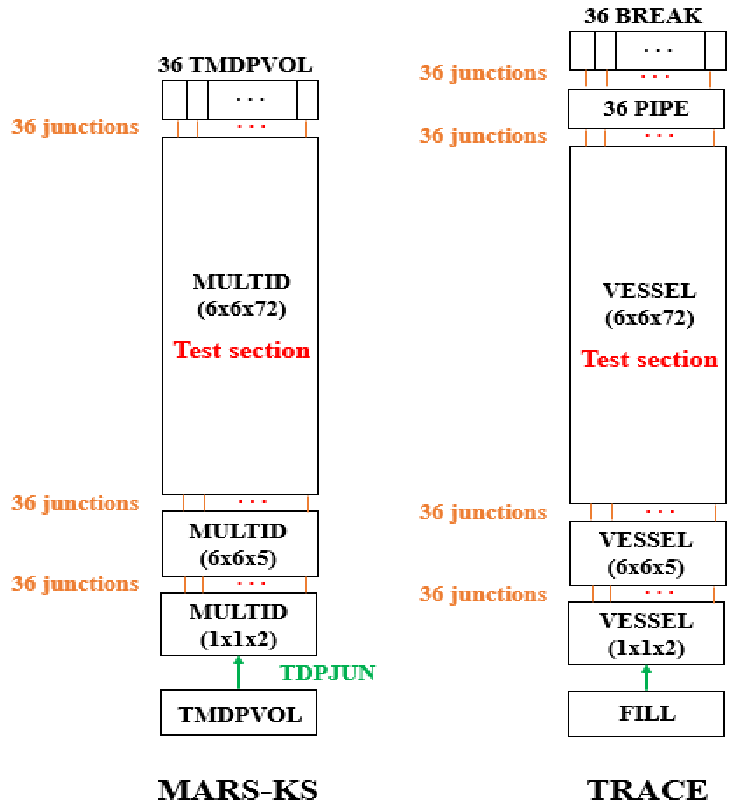

Parameter (unit)		Corner	Side	Center
Volume fraction (porosity)		6.6287×10^{-1}	6.1203×10^{-1}	5.5353×10^{-1}
Gap area fraction	Facing Corner	3.4483×10^{-1}	3.4483×10^{-1}	2.4603×10^{-1}
	Facing Center		2.4603×10^{-1}	
K-factor of spacer grid	Simple	0.4		
	Mixing vane	1.0		
	Non-mixing vane	0.7		

3 RESULTS AND DISCUSSION

3.1 Assessment Results

3.1.1 GE 3X3

A total of 13 test cases, outlined in Table 3-1, were computed using the 3D models of both system codes. The calculated equilibrium quality and mass flux results from both codes were compared against experimental data.

Figure 3-1 displays the calculated equilibrium quality at the exit of specific subchannels. In general, both codes tended to overestimate the quality at the corner, whereas the results at the side and center mostly fell within the experimental error bounds. This discrepancy suggests that both codes predicted significantly more vapor at the corner than what was measured. Consequently, due to this overestimation at the corner, both codes underestimated the mass flux since they predicted much vapor than the experiment at the corner, as illustrated in Figure 3-2.

As outlined in Table 3-2, the root mean square error (RMSE) results notably indicate that TRACE significantly overestimated vapor at the corner compared to MARS-KS. Illustrated in Figure 3-3 and 3-4, the overprediction tendency of TRACE was attributed to its underestimation of crossflow at the corner. This finding suggests that TRACE tended to concentrate vapor at the corner, while MARS-KS exhibited a tendency to disperse vapor toward the peripheral channels. Additionally, as depicted in Figure 3-5, the comparison of net vapor generation rates calculated by both codes revealed that TRACE overestimated vapor generation at the corner. Consequently, these findings underscore that TRACE predicted a higher void distribution at the corner by calculating larger vapor generation, coupled with constrained crossflows between channels.

Figure 3-6 displayed the results of additional calculations using 4x4 subchannels with the 3D components of both system codes. To minimize the contribution of crossflow to the void distribution calculation, all 16 subchannels were modeled with identical geometry and boundary conditions. Interestingly, the results of the 4x4 subchannels calculations revealed a shift: MARS-KS began to compute a larger vapor generation than TRACE once the influence of crossflow was mitigated. This outcome vividly highlights that TRACE's overestimation of vapor generation at the corner stemmed from restricted crossflow calculations. Therefore, it can be concluded that the substantial disparities in both code predictions fundamentally arose from differences in crossflow calculations.

Table 3-1 Test Cases of the GE 3X3 Experiment [Ref. 8]

Test cases	Power (kW)	Mass flow (kg/s)	Inet subcooling internal energy (kJ/kg)
2B2	532	1.359	914.35
2B3	532	1.372	1010.20
2B4	532	1.372	1140.30
2C1	532	2.717	1130.40
2C2	532	2.738	1181.80
2D1	1064	1.384	660.40
2D3	1064	1.384	974.20
2E1	1064	2.769	931.70
2E2	1064	2.769	1039.40
2E3	1064	2.717	1197.00
2G1	1596	2.743	739.30
2G2	1596	2.769	823.40
2G3	1596	2.743	924.00

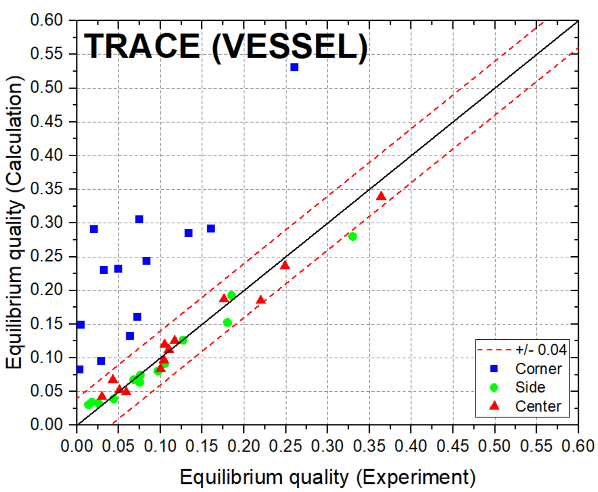

(a) TRACE

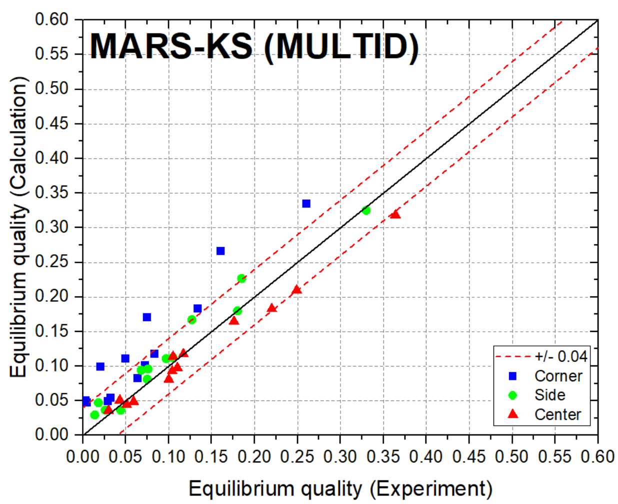

(b) MARS-KS

Figure 3-1 Calculated Results of the GE3X3 Test - Equilibrium Quality

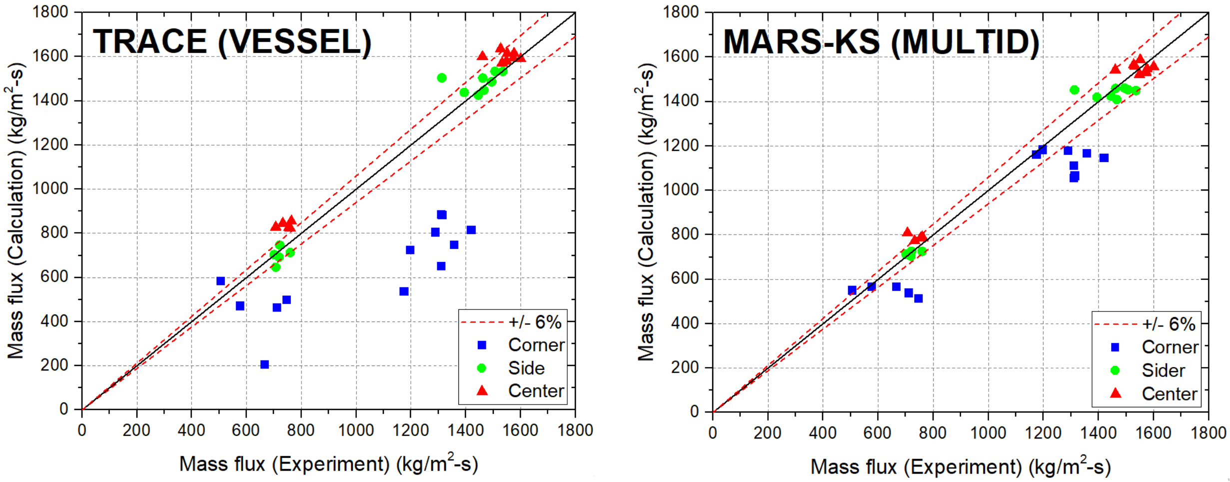

(a) TRACE

(b) MARS-KS

Figure 3-2 Calculated Results of the GE3X3 Test – Mass Flux

Table 3-2 Root Mean Square Error of the GE 3X3 Calculation by System Codes

Figure of merit		RMSE [CAL - EXP]	
		TRACE (VESSEL)	MARS-KS (MULTID)
Equilibrium quality	Corner	0.17231	0.06026
	Side	0.01862	0.02153
	Center	0.01664	0.02166
Figure of merit		RMSE [(CAL – EXP)/EXP (%)]	
		TRACE (VESSEL)	MARS-KS (MULTID)
Mass flux	Corner	40.995	16.172
	Side	5.3478	4.0168
	Center	8.8732	5.1730

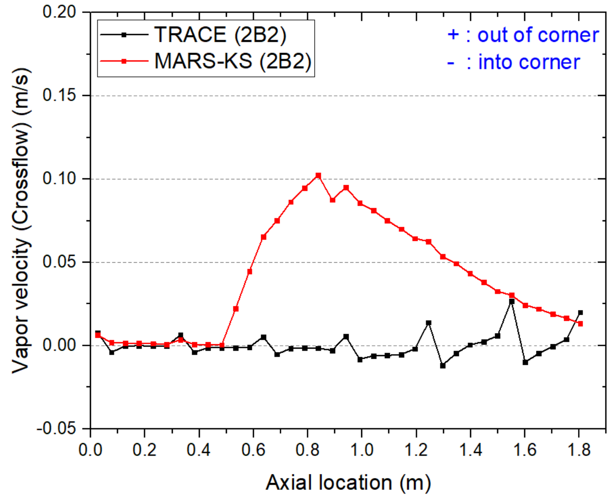

(a) Vapor crossflow velocity (2B2)

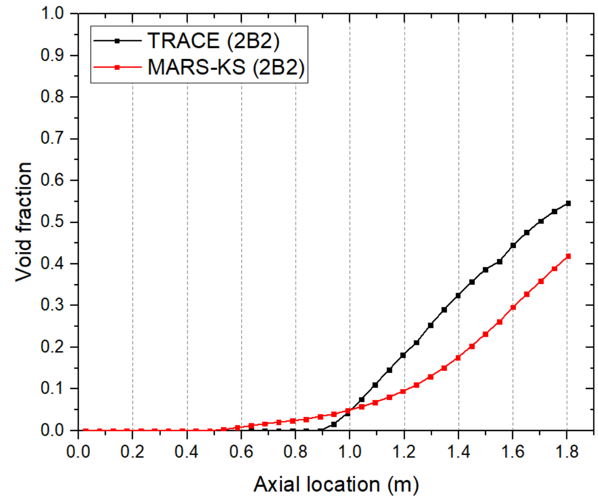

(b) Void fraction (2B2)

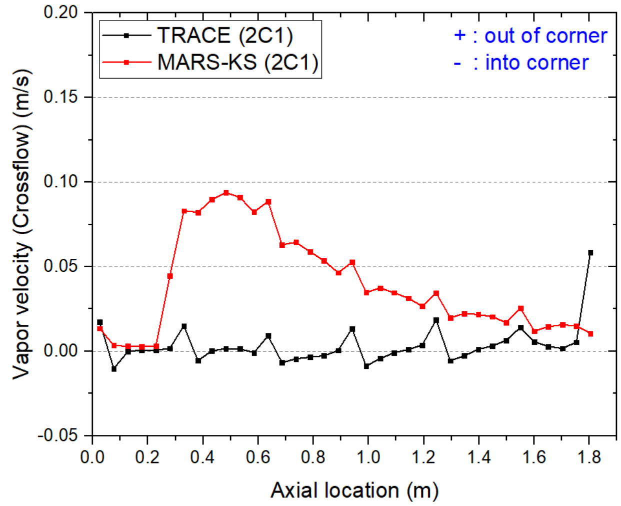

(c) Vapor crossflow velocity (2C1)

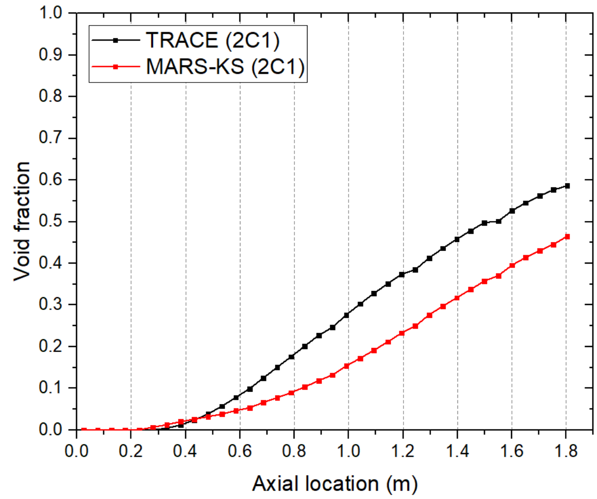

(d) Void fraction (2C1)

Figure 3-3 Results Comparison – Axial Distribution of Void Fraction and Vapor Crossflow Velocity at the Corner (Low and High Flow Conditions at Low Heater Power)

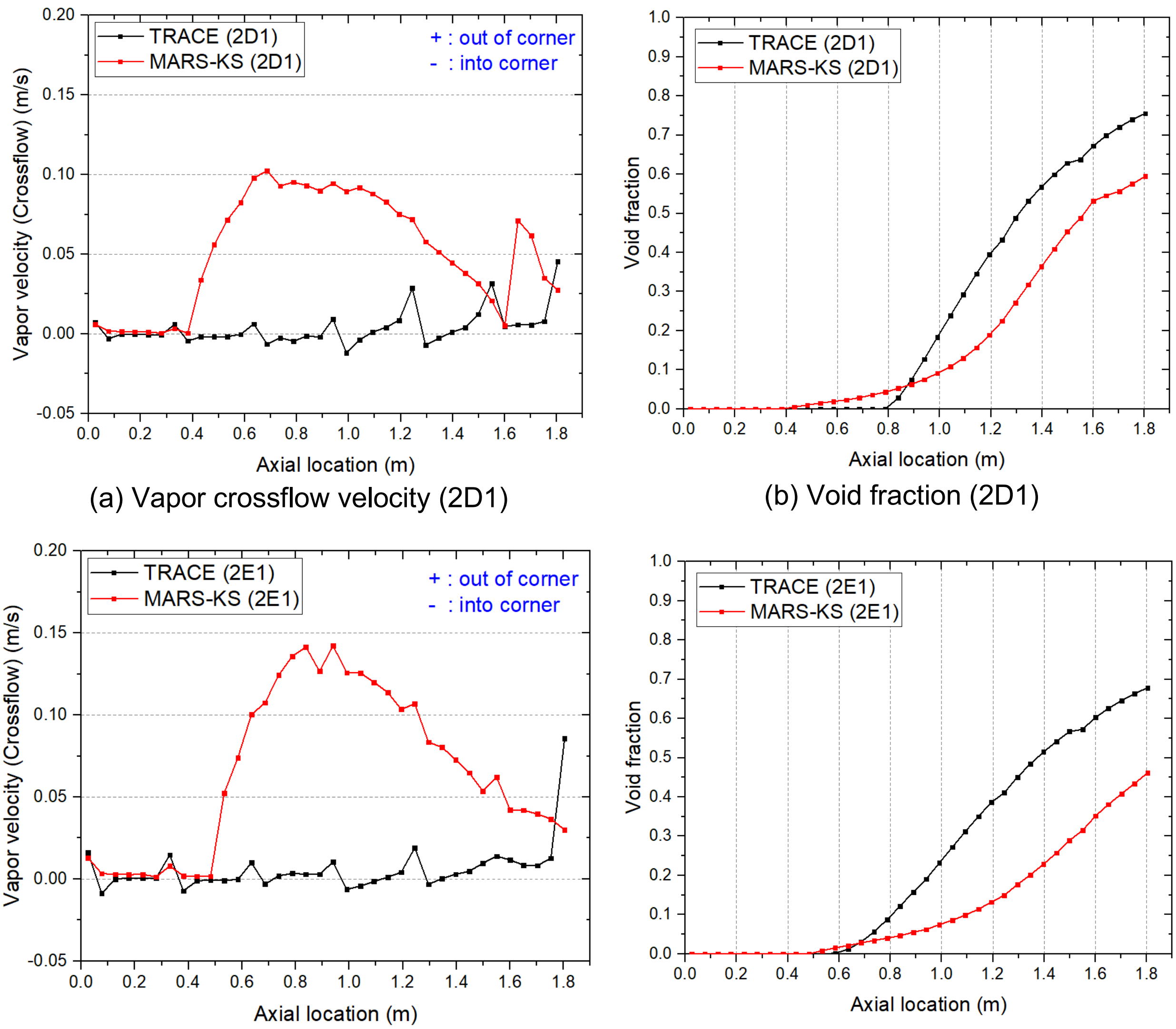

(a) Vapor crossflow velocity (2D1)

(b) Void fraction (2D1)

(c) Vapor crossflow velocity (2E1)

(d) Void fraction (2E1)

Figure 3-4 Results Comparison – Axial Distribution of Void Fraction and Vapor Crossflow Velocity at the Corner (Low and High flow Conditions at High Heater Power)

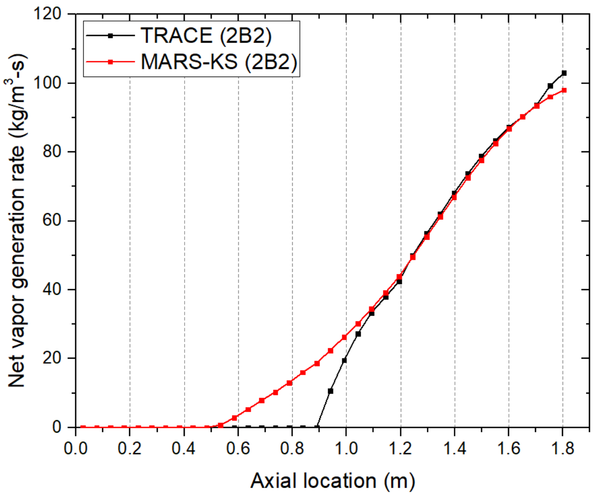

(a) Vapor generation (2B2)

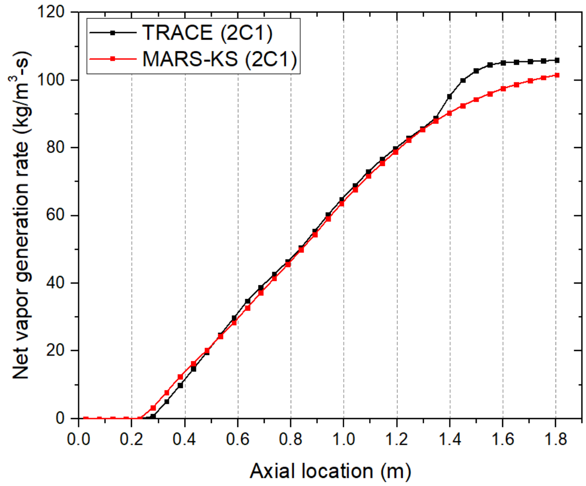

(b) Vapor generation (2C1)

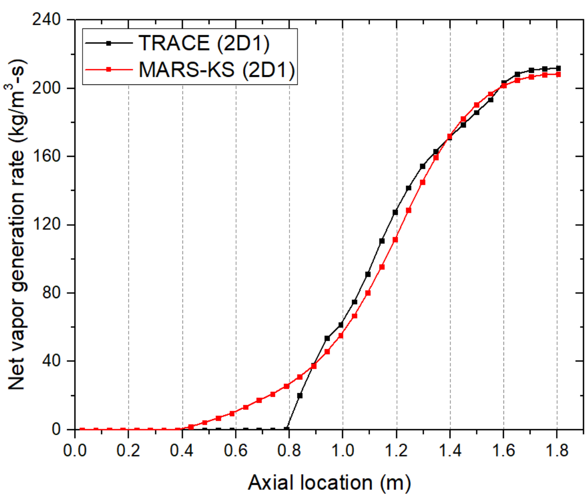

(c) Vapor generation (2D1)

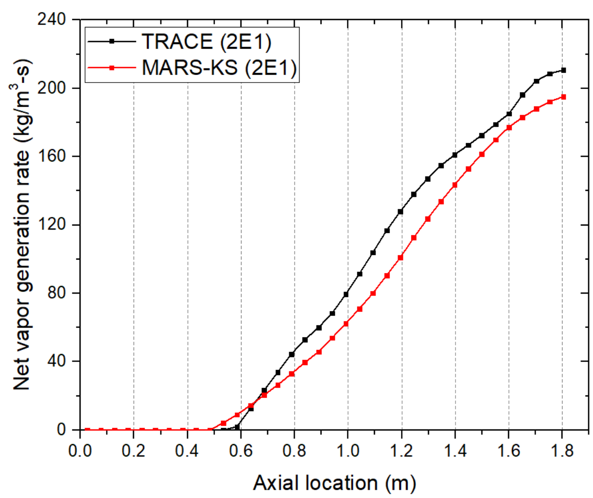

(d) Vapor generation (2E1)

Figure 3-5 Results Comparison – Net Vapor Generation Rate at the Corner

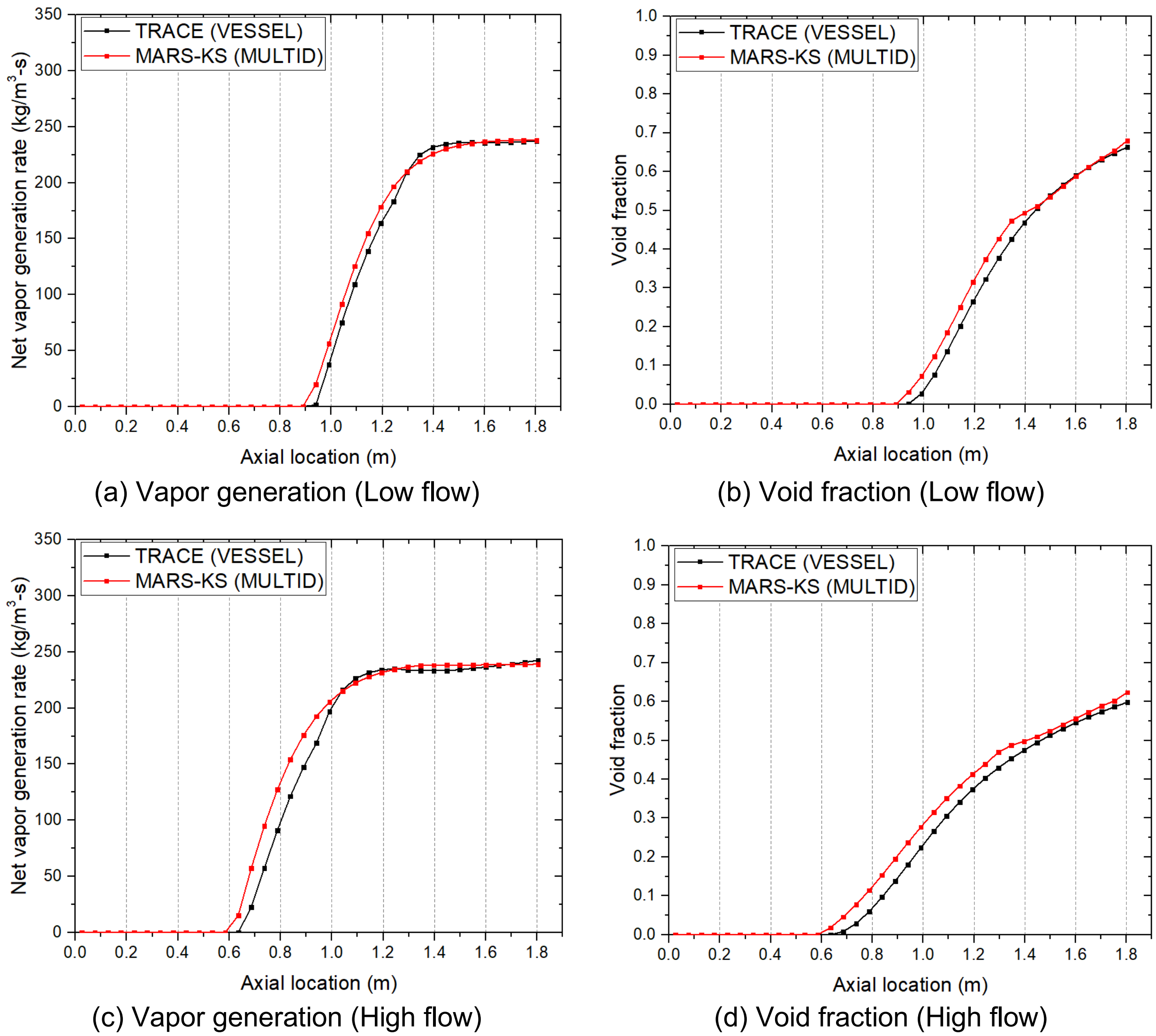

(a) Vapor generation (Low flow)
(b) Void fraction (Low flow)
(c) Vapor generation (High flow)
(d) Void fraction (High flow)

Figure 3-6 Results Comparison – 4x4 Subchannels with the Same Geometry and Boundary Conditions

3.1.2 PSBT Bundle

A total of 148 test cases were computed for both B5 and B6 tests using the 3D models of both system codes. The calculated void fraction results, averaged over the four central subchannels, from both codes were compared against the experimental data.

Figure 3-7 presents the results of void fraction calculations by both 3D models. Notably, TRACE exhibited a significant overprediction tendency, while MARS-KS mostly underestimated the results compared to the results of TRACE. The results of RMSE results in Table 3-3 statistically indicate that MARS-KS predicted the void fraction within the experiment's error bounds, whereas TRACE significantly overestimated the void fraction compared to the measurements.

Figure 3-8 distinctly illustrates TRACE’s significantly overestimation of the vapor at the central channels in contrast to MARS-KS. Moreover, TRACE showed a tendency for restricted crossflows, whereas MARS-KS calculated much larger crossflows that dispersed the vapor toward the peripheral channels, as depicted in Figure 3-9.

Figure 3-10 delineates the reason behind TRACE's restricted crossflow calculations, highlighting its calculation of significantly larger interfacial drag on the crossflow. As specified in Table 3-4, TRACE applied the drift flux model for both vertical and horizontal flows, resulting in substantial interfacial drag in crossflow similar to that in vertical flow [6]. Conversely, MARS-KS utilized the drift flux model solely for vertical flows and employed the drag coefficient model for horizontal flows [7]. Consequently, this led to smaller interfacial drag than TRACE and consequently increased crossflows between channels.

Figure 3-11 clearly shows the impact of interfacial drag on crossflow calculations. When employing the same interfacial drag model as TRACE, the void fraction calculation of MARS-KS generally increased. The RMSE results in Table 3-5 clearly indicate that once the interfacial drag was enlarged, MARS-KS exhibited similar predictability to TRACE under low void conditions below 30%. However, such significant changes were not observed under high void conditions exceeding 30%. The figure reveals that in the high void region, MARS-KS maintained similar crossflow behaviors to its original calculations, even with the application of the same interfacial drag model as TRACE. This discrepancy stemmed from differing calculations of interfacial friction coefficients, where the modified MARS-KS displayed smaller interfacial friction than the expected values, as per TRACE.

This discrepancy in smaller interfacial friction calculations was attributed to a limitation in MARS-KS, wherein it multiplied the junction area ratio to the interfacial friction coefficients as described below.

$$Area\ ratio = \frac{A_{jun}}{(\Delta x)_{From} + (\Delta x)_{To}}\left[\frac{(\Delta x)_{From}}{(A_{vol})_{From}} + \frac{(\Delta x)_{To}}{(A_{vol})_{To}}\right] \quad \textbf{(3-1)}$$

Since the specified gap area was smaller than the volume-averaged area of the connected subchannels, the multiplication of the area ratio reduced the interfacial friction coefficients. Figure 3-12 shows the results when the area ratio was removed for the crossflow junctions. As depicted in the figure, the interfacial friction coefficients drastically increased in comparison to the results of TRACE. Moreover, in some instances, these coefficients were notably larger than those computed by TRACE.

The drift flux model of TRACE employs the minimum values of drift velocities calculated by both the Ishii model (Eq. **3-2**) and the Kataoka-Ishii model (Eq. **3-3**), respectively.

$$v_{gj} = \sqrt{2}\left[\frac{\sigma \mathrm{g}(\rho_f - \rho_g)}{\rho_f^2}\right]^{0.25}, \tag{3-2}$$

$$v_{gj} = 0.0019\left[\frac{D_h}{\sqrt{\sigma/\mathrm{g}(\rho_f - \rho_g)}}\right]^{0.809}\left[\frac{\mu_f}{\left(\rho_f \sigma\sqrt{\sigma/\mathrm{g}(\rho_f - \rho_g)}\right)^{0.5}}\right]^{-0.562}, \tag{3-3}$$

In Figure 3-13, the fluid properties utilized in these correlations were compared across various system pressure conditions within this experiment. The figure distinctly highlights that the discrepancy arose from the surface tension calculations, particularly evident at high-pressure conditions exceeding 10 MPa, where both codes showcased substantial differences. At high-pressure conditions, TRACE maintained a constant surface tension value, whereas MARS-KS computed progressively smaller results as the system pressure increased. The figure clearly indicated that the overestimation of interfacial friction coefficients by the modified MARS-KS (without the area ratio restriction) corresponded to the smaller surface tension calculations observed at high-pressure conditions.

Nevertheless, even after computing interfacial friction without the area ratio restriction, the void fraction continued to be underestimated compared to the results of TRACE at the high void region. In this domain, the results of the annular-mist model prevailed over the drift flux calculations, as TRACE employed a weighting function for the interfacial drag calculations as described below.

$$C_i = \sqrt{(C_i)^2_{bby-slug} + (C_i)^2_{ann-mist}} \tag{3-4}$$

For the annular-mist model (Eq. **3-5**), TRACE utilized the drop drag model of Ishii-Chawla (Eq. **3-6**) combined with the film friction model of Wallis (Eq. **3-7**).

$$(C_i)_{ann-mist} = (C_i)_{drop} + (C_i)_{film} \tag{3-5}$$

$$\begin{aligned}(C_i)_{drop} &= \frac{\rho_g}{2} A'''_{i,drop} C_d \\ &= \rho_g \frac{3\alpha_d}{4 d_d}\left[\frac{24}{Re_d}\{1 + 0.1(Re_d)^{0.75}\}\right],\end{aligned} \tag{3-6}$$

$$
\begin{aligned}
(C_i)_{film} &= \frac{\rho_g}{2} A'''_{i,film}\left[0.005\left(1+75\alpha_{film}\right)\right] \\
&= 2\sqrt{\alpha_g}\frac{\rho_g}{D_h}\left[0.005\left(1+75\alpha_{film}\right)\right]
\end{aligned}
\quad \textbf{(3-7)}
$$

As depicted in Figure 3-14, it was observed that TRACE overestimated the interfacial friction coefficient for the annular-mist model; the drop drag term was overestimated compared to the results of modified MARS-KS, while the film friction term showed no significant difference. This overestimation in the drop drag term stemmed from TRACE's overcalculation of Wallis drag coefficients. Specifically, TRACE underestimated the drop Reynolds number in comparison to the modified MARS-KS, as illustrated in Figure 3-15. However, since the drop Reynolds number is computed based on the phasic relative velocity, these findings suggest that TRACE's overestimation in the drop drag model was primarily influenced by restricted crossflow calculations. This implies the existence of other factors contributing to such crossflow restrictions by TRACE in the high void region.

Consequently, this assessment definitively highlights the substantial sensitivity of code predictions to interfacial drag calculations. The results illustrate a direct impact of interfacial drag models on crossflow calculations, ultimately altering the phasic distribution within the bundle. This underscores the fundamental influence of crossflow calculations on code predictions at the subchannel-scale level, emphasizing their paramount importance in accurate predictions.

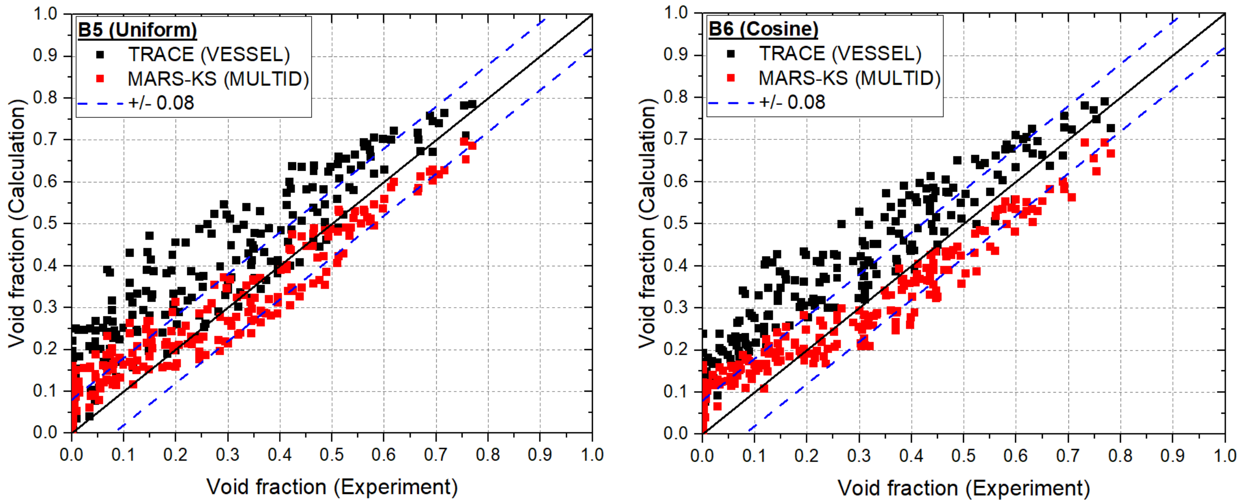

(a) B5 (b) B6

Figure 3-7 Calculated Results of PSBT Bundle Test – Void Fraction

Table 3-3 Root Mean Square Error of PSBT Calculation by System Codes

B5		RMSE [CAL - EXP]	
		TRACE (VESSEL)	MARS-KS (MULTID)
Void fraction	< 30%	0.15535	0.07907
	> 30%	0.10185	0.06365
	ALL	0.13644	0.07328
B6		RMSE [CAL - EXP]	
		TRACE (VESSEL)	MARS-KS (MULTID)
Void fraction	< 30%	0.15001	0.07228
	> 30%	0.10025	0.07658
	ALL	0.13062	0.07419

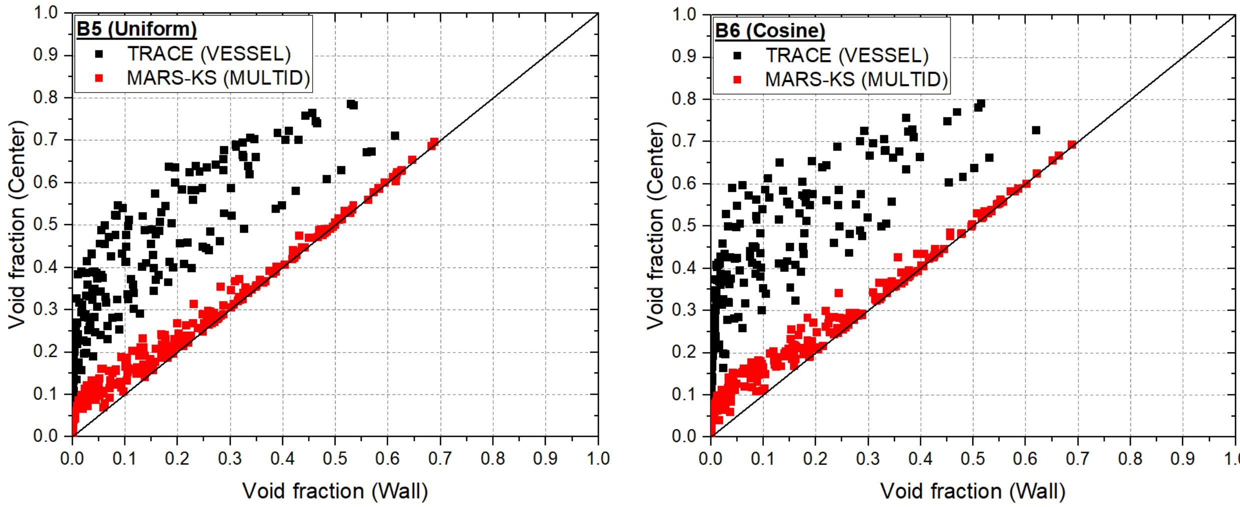

(a) B5 (b) B6

Figure 3-8 Results Comparison – Void Distribution Over the Cross-Section of Test Section

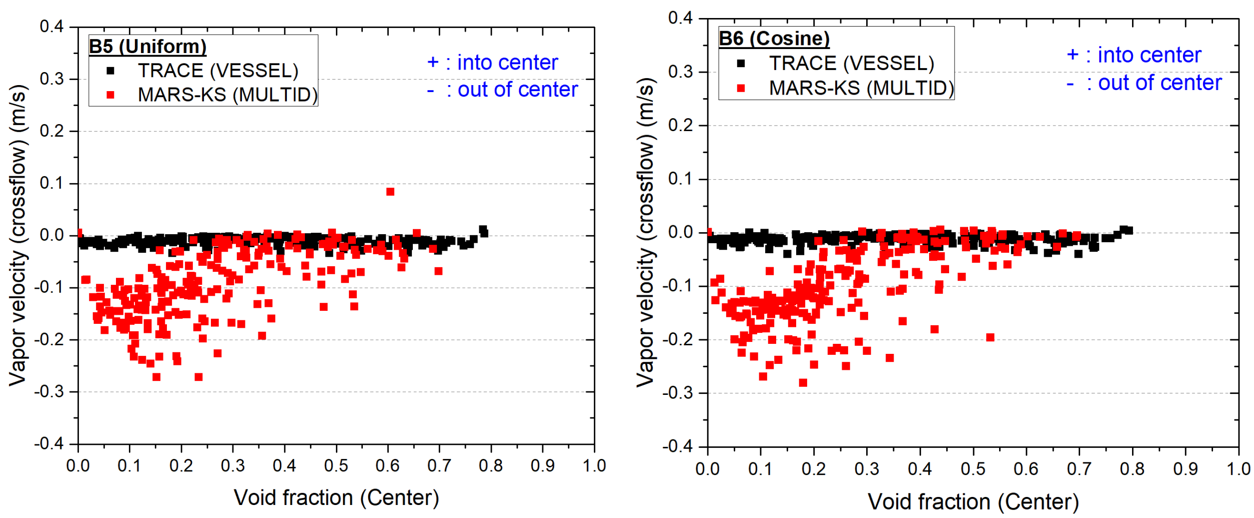

(a) B5 (b) B6

Figure 3-9 Results Comparison – Vapor Crossflow Velocity at the Central Channels

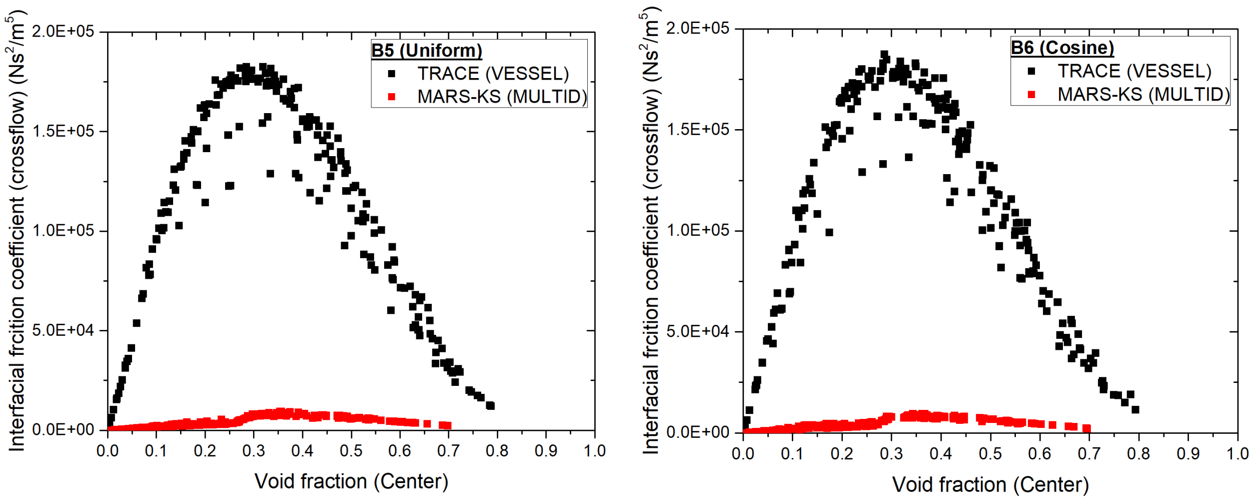

(a) B5 (b) B6

Figure 3-10 Results Comparison – Interfacial Friction Coefficient at the Crossflow Junctions of Central Channels

Table 3-4 Comparison of Interfacial Drag Models in Both System Codes

Flow type	Flow regime	Models	
		TRACE	MARS-KS
Vertical	Bubbly	Churn-Turbulent (Ishii)	EPRI ($G \geq 100\, kg/m^2s$) Zuber-Findley ($G < 100\, kg/m^2s$)
	Slug	Kataoka-Ishii	
	Annular-mist	Drop drag (Ishii-Chawla) + Film drag (Wallis)	Drag coefficient (Ishii-Chawla)
Crossflow	Bubbly	Churn-Turbulent (Ishii)	Drag coefficient (Ishii-Chawla)
	Slug	Kataoka-Ishii	
	Annular-mist	Drop drag (Ishii-Chawla) + Film drag (Wallis)	

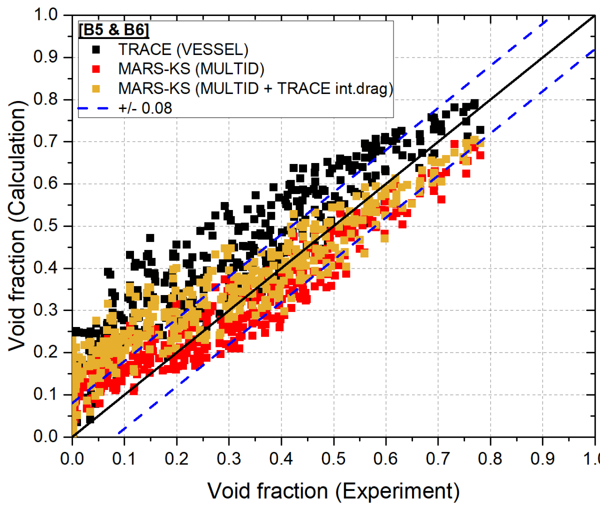

(a) Void fraction

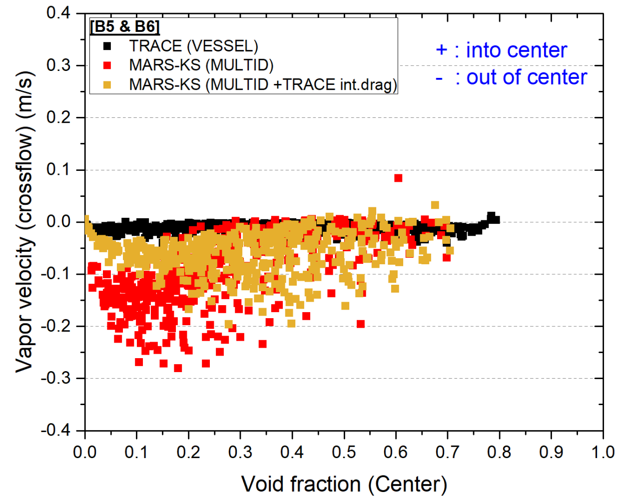

(b) Vapor crossflow velocity

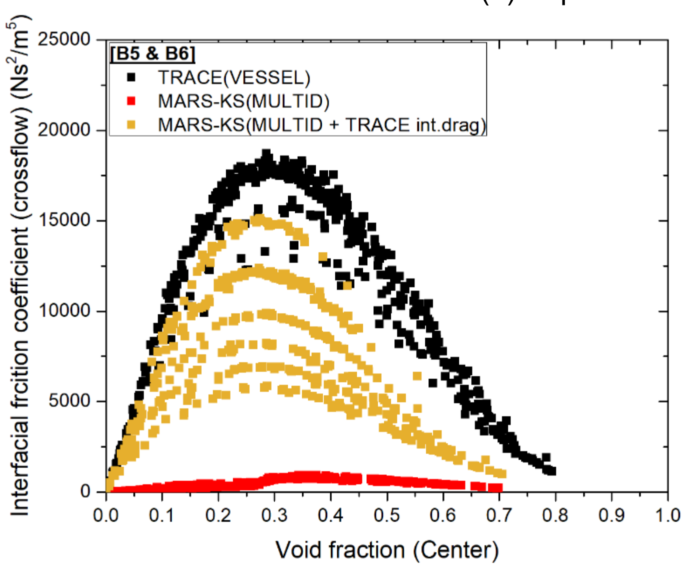

(c) Interfacial friction coefficient

Figure 3-11 Results Comparison – Change of Void Prediction with TRACE Drag Model Interfacial

Table 3-5 Change of the Root Mean Square Error Results with Interfacial Drag Models for PSBT Calculation

B5		RMSE [CAL - EXP]		
		TRACE (VESSEL)	MARS-KS (MULTID)	MARS-KS (MULTID + TRACE int.drag)
Void fraction	< 30%	0.15535	0.07907	0.12629
	> 30%	0.10185	0.06365	0.05116
	ALL	0.13644	0.07328	0.10298
B6		RMSE [CAL - EXP]		
		TRACE (VESSEL)	MARS-KS (MULTID)	MARS-KS (MULTID + TRACE int.drag)
Void fraction	< 30%	0.15001	0.07228	0.11573
	> 30%	0.10025	0.07658	0.05179
	ALL	0.13062	0.07419	0.09335

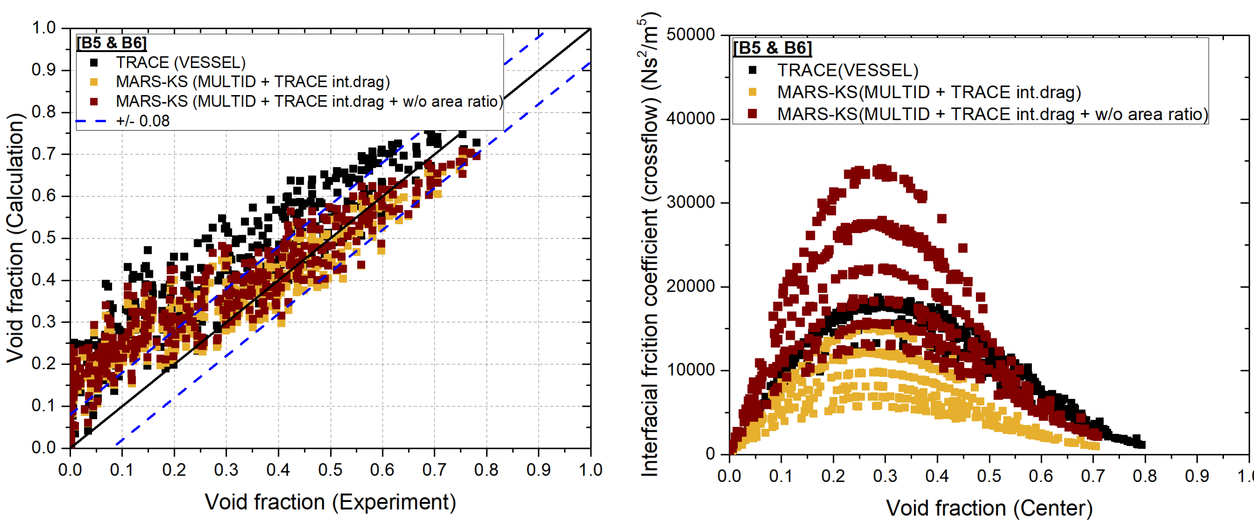

(a) Void fraction (b) Interfacial friction coefficient

Figure 3-12 Results Comparison – without Restriction on Interfacial Friction For Crossflow Junctions Using TRACE Interfacial Drag Model

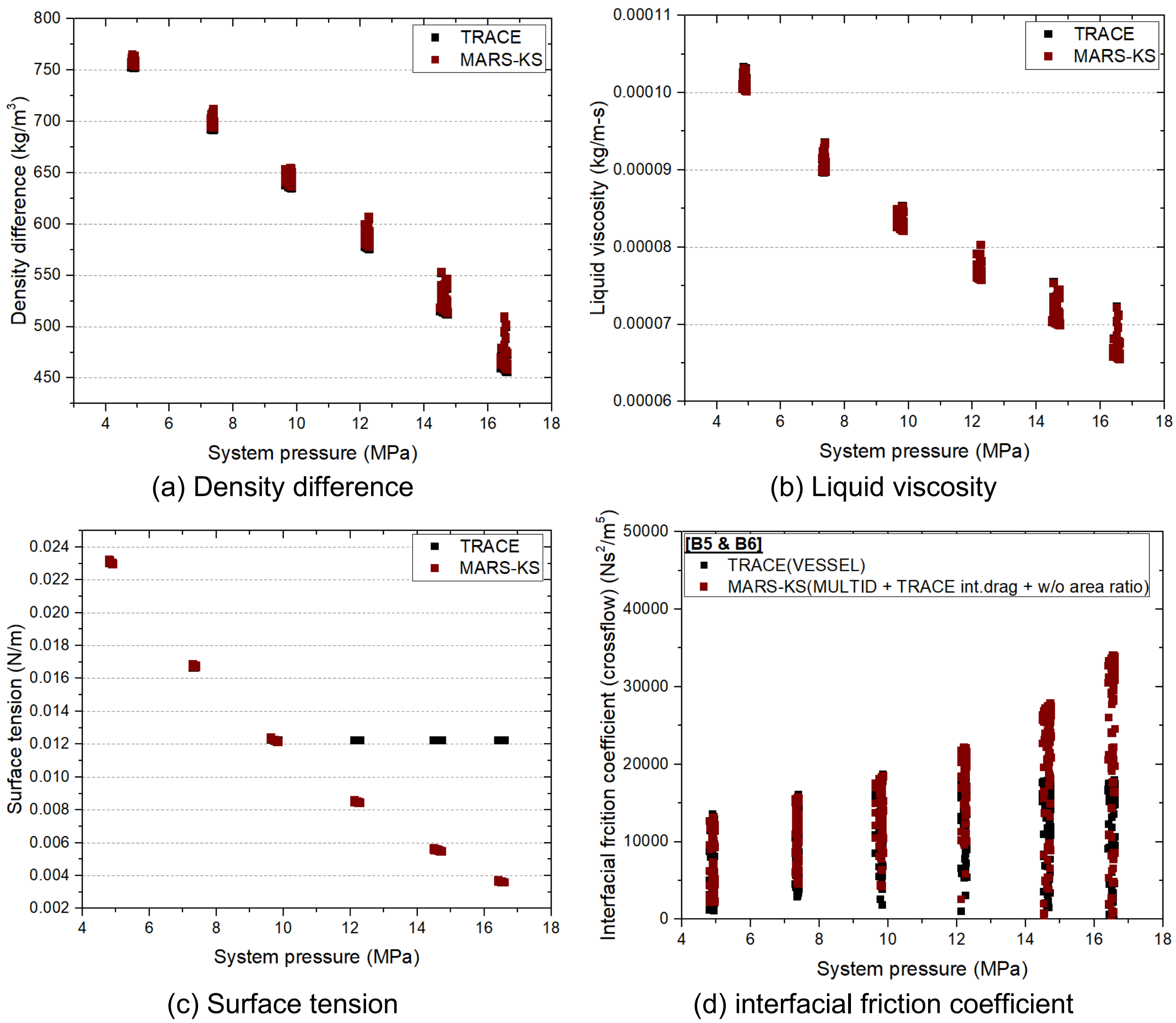

(a) Density difference

(b) Liquid viscosity

(c) Surface tension

(d) interfacial friction coefficient

Figure 3-13 Results Comparison – Fluid Properties Used in Drift Flux Model of TRACE

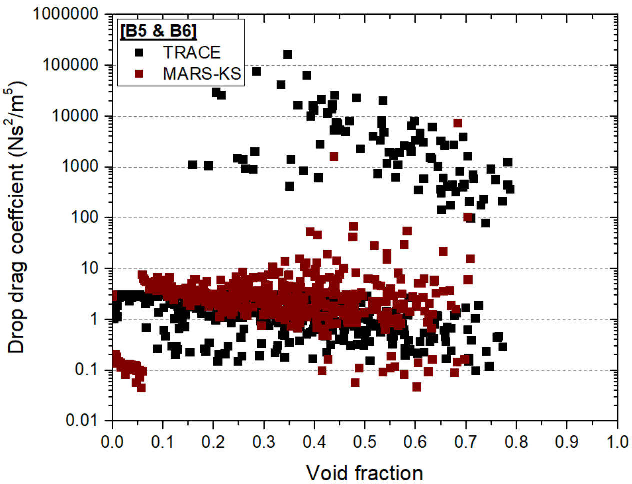

(a) Drop drag term, $(C_i)_{drop}$

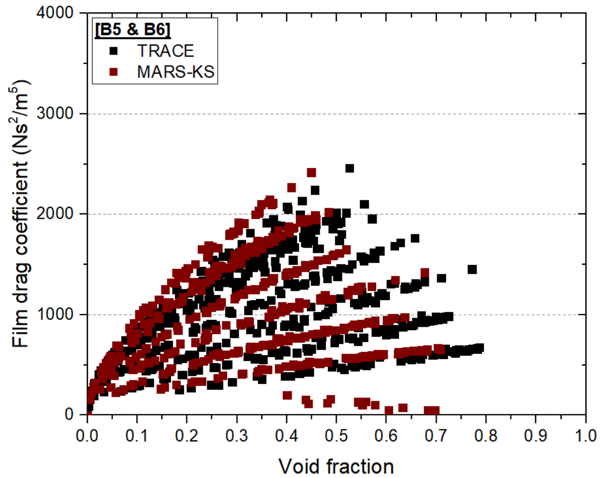

(b) Film friction term, $(C_i)_{film}$

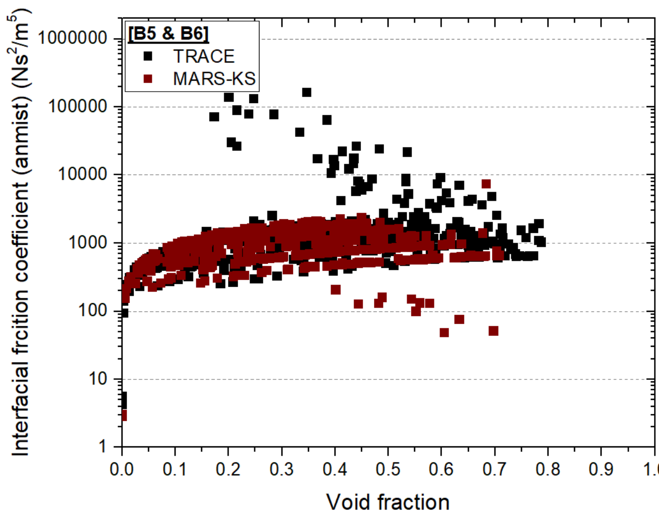

(c) Interfacial friction coefficient of annular-mist model, $(C_i)_{ann-mist}$

Figure 3-14 Results Comparison – Annular-Mist Interfacial Friction Model of TRACE

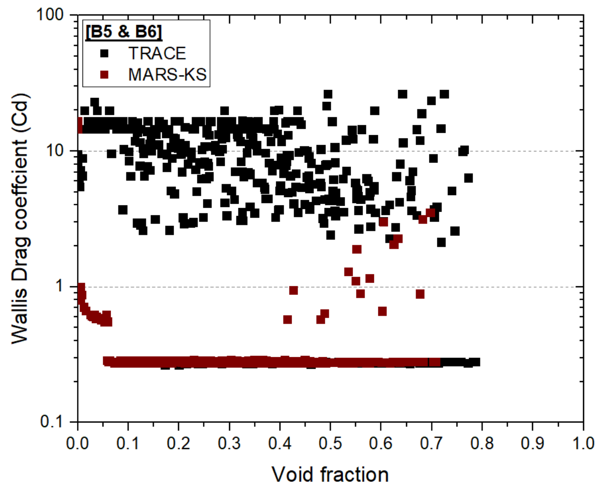

(a) Wallis drag coefficient

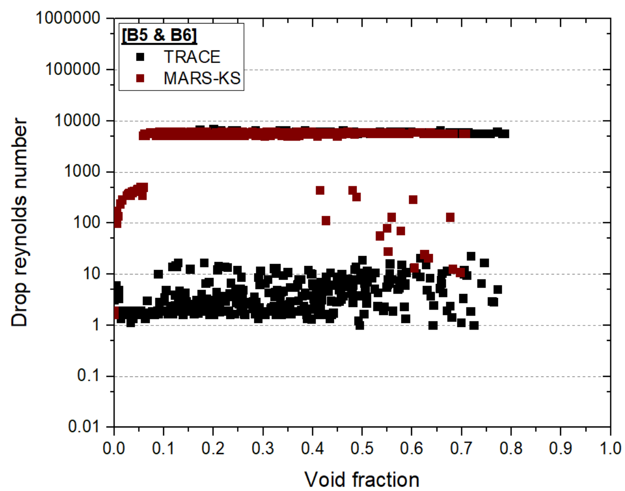

(b) Drop Reynolds number

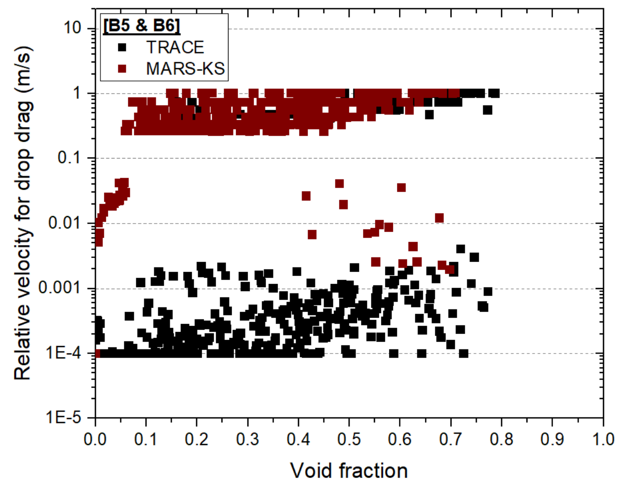

(c) Relative velocity for drop drag

Figure 3-15 Results Comparison – Drop Drag Model of TRACE

3.2 Key Findings from the Assessment

Figure 3-16 illustrates the quality distribution within the GE 3X3 test conditions. The measured data distinctly displays a higher vapor concentration at the center compared to the corner. However, the code calculations estimated a higher vapor concentration at the corner instead.

Table 3-6 outlines the power-to-flow ratio conditions at the measured subchannels of the experiment. The results indicate that the corner had the highest power-to-flow ratio due to reduced coolant flow caused by a significant pressure drop in comparison to the other locations. Interestingly, despite these conditions, the experiment reported lower enthalpy at the corner than in the bulk conditions. The experimental explanation for this outcome suggested that crossflow diverted the vapor towards the center, where the flow resistance was comparatively lower. Similar phenomena have been documented in related studies [10-12]. Consequently, these findings strongly suggest inadequate predictions by the 3D components of both system codes regarding the experiment's crossflow behavior.

While the initial development of system codes did not cater to such intricate small-scale analyses, recent regulatory focus on high-burnup fuels necessitates a detailed examination, including the context surrounding the targeted hot pin. Therefore, there is a pressing need for system codes to accommodate these specifics, prompting an essential improvement in the crossflow model. To effectively capture crossflow behaviors, integrating a turbulence model suitable for subchannel-scale analysis becomes imperative.

At the subchannel-scale level, the presence of a rod bundle induces substantial flow disturbances, fostering notable secondary flows between channels [13-18]. These secondary flows trigger shifts in vapor and liquid distribution, consequently altering the phasic distribution within the bundle. Hence, state-of-the-art subchannel analysis codes predominantly incorporate the subchannel mixing model to address these secondary flow effects [19-20]. This model operates by accounting for net mass transfer between adjacent channels based on void distribution. The impact of these secondary flows in subchannel-scale problems is well-documented, with reports indicating significant differences in results when utilizing or omitting this model [21].

Figure 3-17 and Figure 3-18 illustrate the impact of enhancing the turbulence model, specifically the introduction of the subchannel mixing model in MARS-KS, on both separate effect tests. These figures depict significant improvements in the overall code predictions following the integration of the subchannel mixing model. Notably, the GE 3X3 experiment displayed a more accurate prediction of quality distribution—a capability not presented in the original calculations. Moreover, in the case of the PSBT experiment, the enhanced model exhibited a reduction in code results within the experimental error range at low void regions by promoting increased net mixing towards peripheral channels. Simultaneously, at high void regions, there was an observed augmentation in results with shifts of vapor towards central channels. The summarized RMSE results in Table 3-7 further support these findings, emphasizing a substantial enhancement in the overall predictability of MULTID in MARS-KS due to the application of the subchannel mixing model, remarkably. Therefore, these results clearly imply that the subchannel mixing model is required for the system codes to implement the crossflow behavior considered at the subchannel-scale level.

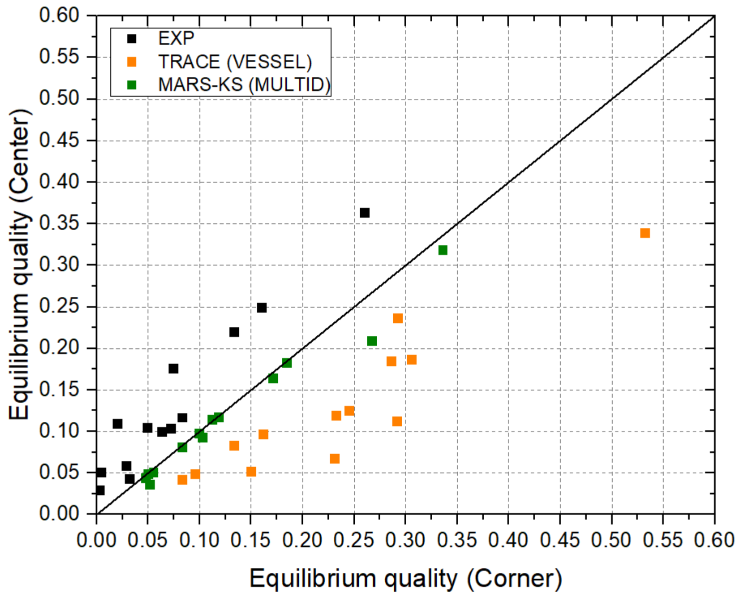

Figure 3-16 Results Comparison – GE 3X3 Quality Distribution

Table 3-6 Power-to-Flow Ratio Conditions at the Measured Subchannels of the GE 3X3 Experiment

Test cases	Power-to-Flow Raito (kW s kg)		
	Corner	Side	Center
2B2	580.07	355.50	432.18
2B3	392.34	349.46	447.96
2B4	411.77	358.24	416.75
2C1	223.60	173.74	216.69
2C2	222.92	180.17	204.01
2D1	1015.43	661.47	839.48
2D3	880.67	696.31	829.03
2E1	454.28	336.14	401.68
2E2	412.59	343.63	395.56
2E3	447.20	342.67	414.54
2G1	733.94	574.03	613.10
2G2	647.35	500.12	619.59
2G3	748.33	490.84	603.60

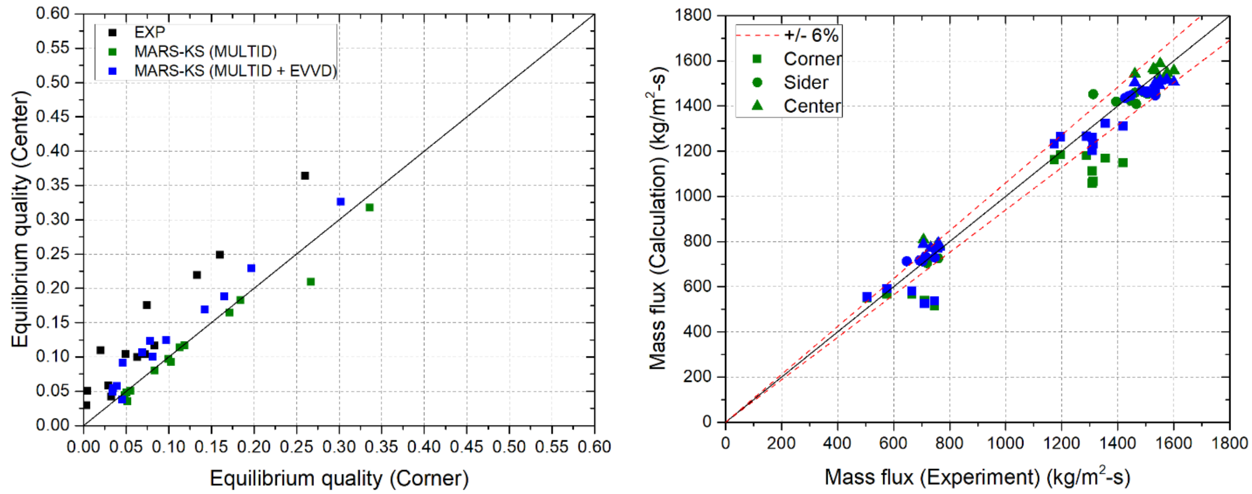

(a) Quality distribution (b) Mass flux

Figure 3-17 Influence of Crossflow Improvement by Subchannel Mixing Model – GE 3X3 Experiment

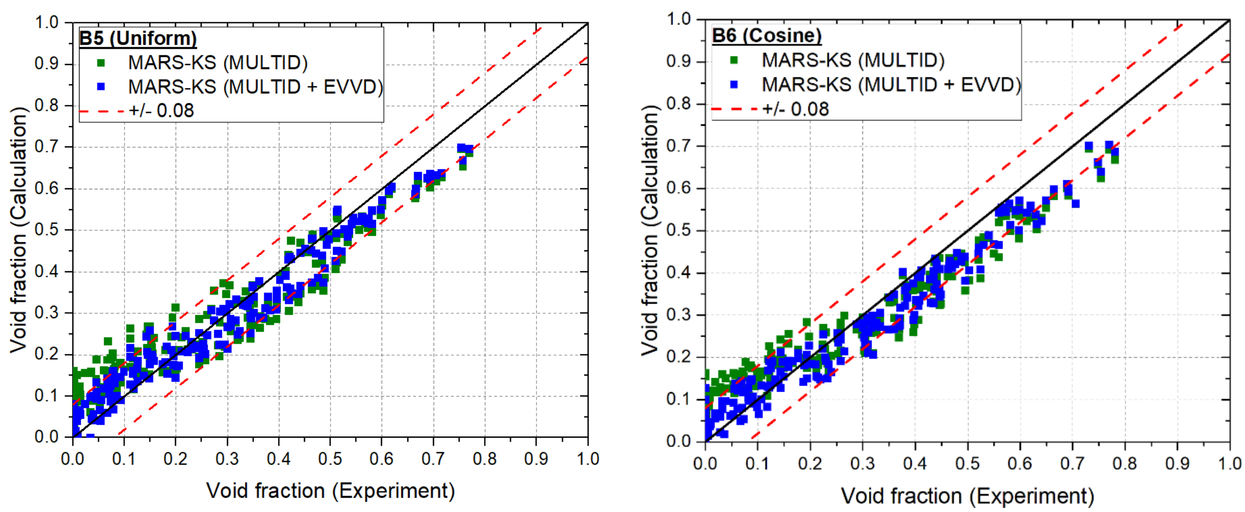

(a) B5 (b) B6

Figure 3-18 Influence of Crossflow Improvement by Subchannel Mixing Model – PSBT Bundle Experiment

Table 3-7 Change of the Root Mean Square Error Results with Crossflow Improvement

GE 3X3		RMSE [CAL - EXP]		
		TRACE (VESSEL)	MARS-KS (MULTID)	MARS-KS (MULTID + EVVD)
Equilibrium quality	Corner	0.17231	0.06026	0.03424
	Side	0.01862	0.02153	0.02005
	Center	0.01664	0.02166	0.01664
GE 3X3		RMSE [(CAL – EXP)/EXP (%)]		
		TRACE (VESSEL)	MARS-KS (MULTID)	MARS-KS (MULTID + EVVD)
Mass flux	Corner	40.995	16.172	12.284
	Side	5.3478	4.0168	3.9116
	Center	8.8732	5.1730	4.7754
PSBT (B5 & B6)		RMSE [CAL - EXP]		
		TRACE (VESSEL)	MARS-KS (MULTID)	MARS-KS (MULTID + EVVD)
Void fraction	< 30%	0.15279	0.07586	0.0418
	> 30%	0.10102	0.07069	0.0611
	ALL	0.13356	0.07373	0.0508

4 CONCLUSIONS

The assessment of 3D components in the TRACE V5.0 patch 7 and MARS-KS 2.0 system codes was carried out using two SETs, namely GE 3X3 and PSBT bundle experiments. The assessment results revealed shortcomings in both codes' predictions of the experiments. Particularly, TRACE significantly overestimated vapor as compared to MARS-KS, as it computed excessive interfacial drag on the crossflows. This excessive drag hindered net mixing between channels, leading to vapor confinement within individual subchannels in the bundle.

TRACE tended to overestimate interfacial drag for crossflows by applying the drift flux model, similar to vertical flows. Meanwhile, MARS-KS generated relatively smaller interfacial drag than TRACE, employing the drag coefficient model for crossflow calculations. This sensitivity in code predictions was evident as MARS-KS also began to overcalculate void fraction when integrating TRACE's model, leading to large interfacial drag in crossflow calculations.

These findings strongly suggest that, at the subchannel-scale level, accurate predictions are greatly influenced by crossflow calculations. The subpar predictions of phasic distribution indicate that both codes fell short in representing the necessary crossflow behaviors for solving subchannel-scale problems. Hence, it is evident that improvements to the crossflow models of both codes are imperative for enhanced subchannel-scale analyses.

The original goal of developing system codes did not involve such detailed small-scale analyses. However, recent regulatory focus on high-burnup fuels demands an in-depth examination of factors affecting the specific hot pin area. Therefore, to meet these demands, the system codes need the capacity for this kind of detailed analysis. Therefore, this study proposes enhancing the crossflow models of both system codes by integrating the subchannel mixing model. This enhancement will enable a more comprehensive consideration of crossflow behaviors at the subchannel-scale level.

5 REFERENCES

[1] A. Petruzzi, F. D' Auria, Thermal-hydraulic system codes in nuclear reactor safety and qualification procedures, Sci. Techno. Nucl. Install., 2008.

[2] G.E. Wilson, Historical insights in the development of best estimate plus uncertainty safey analysis, Ann. Nucl. Energy., 52, 2–9, 2013.

[3] I. Clifford, H. Ferroukhi, Assessing the effects of switching from multi-channel to three-dimensional nodalisations of the core in TRACE, Nucl. Eng. Des., 383, 2021.

[4] G. Repetto, C. Dominguez, B. Durville, S. Carnemolla, D. Campello, N. Tardif, M. Gradeck, The R&D PERFROI project on thermal mechanical and thermal hydraulics behaviors of a fuel rod assembly during loss of coolant accident, NURETH-16, Chicago, IL, August 30–September 4, 2015.

[5] P. Gao, B. Zhang, J. Shan, Study on the effect of flow blockage due to rod deformation in QUENCH experiment, Nuclear Engineering and Technology 54, 3154–3165, 2022.

[6] United States Nuclear Regulatory Commission, TRACE V5.0 theory manual, Field equations, solution methods, and physcial models, 2020.

[7] Korea Institute of Nuclear Safety, MARS-KS code manual, Volume Ⅰ: Theory manual, KINS/RR-1822 Vol.1, 2018.

[8] R.T. Lahey Jr., B.S. Shirlakar, D.W. Radcliffe, Two-phase flow and heat transfer in multirod geometries: subchanel and pressure drop measurements in a nine-rod bundle for diabatic and adiabatic conditions, Tech. rep. Gen. Electrics., GEAP-1304, 1970.

[9] A. Rubin, A. Schoedel, M. Avramova, OECD/NRC Benchmark Based on NUPEC PWR Subchannel and Bundle Tests (PSBT), Volume I: Experimental Database and Final Problem Specifications, OECD Nuclear Energy Agency, NEA/NSC/ DOC(2010), 2010.

[10] H. Herkenrath, W. Hufschmidt, U. Jung, F. Weckermann, Experimental investigation of the enthalpy and massflow distribution in 16-rod clusters with BWR-PWR geometries and conditions, EUR 7575 EN., 1981.

[11] M. Sadatomi, A. Kawahara, Y. Sato, Flow redistribtution due to void drift in two-phase flow in a multiple channel consisting of tow subchannels, Nucl. Eng. Des., 148, 463–474, 1994.

[12] M. Sharma, A.K. Nayak, Experimental investigation of void drift in simulated subchannels of a natural circulation pressure tube type BWR, Nuclear Technology, 197, 2017.

[13] D.S. Rowe, B.M. Johnson, J.G. Knudsen, Implications concerning rod bundle crossflow mixing based on measurements of turbulent flow structure, Int. J. Heat Mass Tran., 17, 404–419, 1974.

[14] K.J. Petrunik, Turbulent Mixing Measurements for Single Phase Air, Single Phase Water, and Two-phase Air-Water Flows in Adjacent Rectangular Subchannels, Master Thesis, Chemical Engineering, Master Thesis, Chemical Engineering, University of Windsor, Canada, 1968.

[15] F.B. Walton, Turbulent Mixing Measurements for Single Phase Air, Single Phase Water, and Two-phase Air-Water Flows in Adjacent Triangular Subchannels, Master Thesis, Chemical Engineering, University of Windsor, Canada, 1969.

[16] F.S. Castellena, W.T. Adams, J.E. Casterline, Single-phase subchannel mixing in a simulated nuclear fuel assembly, Nucl. Eng. Des., 26, 242–249, 1974.

[17] D.S. Rowe, C.W. Angle, Crossflow mixing between parallel flow channels during boiling, Part II Measurement of flow and enthalpy in two parallel channels, BNWL371 PT2, 1967.

[18] M. Sadatomi, A. Kawahara, K. Kano, Y. Sumi, Single- and two-phase turbulent mixing rate between adjacent subchannels in a vertical 2x3 rod array channel, Int. J. Multiphas. Flow., 30, 481–498, 2004.

[19] N.E. Todreas, M.S. Kazimi, Subchannel analysis, in: Nuclear Systems II – Elements of Thermal Hydraulic Design, Taylor & Francis Group, Boca Raton, FL, pp. 209–284, 1990.

[20] R.T. Lahey, F.J. Moody, Subchannel analysis, in: The Thermal-Hydraulics of A Boiling Water Nuclear Reactor, second ed., American Nuclear Society, pp. 168–184, 1993.

[21] R.K. Salko, T.S. Blyth, C.A. Dances, J.W. Magedanz, C. Jernigan, J. Kelly, A. Toptan, M. Gergar, M.N. Avramova, S. Palmtag, J.C. Gehin, CTF Validation and Verification, US Department of Energy, CASL-U-2016-1113-000, 2016.

NRC FORM 335 (12-2010) NRCMD 3.7 U.S. NUCLEAR REGULATORY COMMISSION **BIBLIOGRAPHIC DATA SHEET** *(See instructions on the reverse)*	1. REPORT NUMBER (Assigned by NRC, Add Vol., Supp., Rev., and Addendum Numbers, if any.) **NUREG/IA-0551**
2. TITLE AND SUBTITLE **Assessment of 3D Components in System Codes Against Separate Effect Tests**	3. DATE REPORT PUBLISHED MONTH: **June** YEAR: **2025**
	4. FIN OR GRANT NUMBER
5. AUTHOR(S) Yunseok Lee*, Taewan Kim*, Jae Soon Kim**, Dong Gu Kang**	6. TYPE OF REPORT Technical
	7. PERIOD COVERED (Inclusive Dates)

8. PERFORMING ORGANIZATION - NAME AND ADDRESS (If NRC, provide Division, Office or Region, U. S. Nuclear Regulatory Commission, and mailing address; if contractor, provide name and mailing address.)

*Incheon National University (INU),
119 Academy-ro, Yeonsu-gu, Incheon 22012, Republic of Korea
**Korea Institute of Nuclear Safety (KINS)
62 Gwahak-ro, Yuseong-gu, Daejeon 34142, Republic of Korea

9. SPONSORING ORGANIZATION - NAME AND ADDRESS (If NRC, type "Same as above", if contractor, provide NRC Division, Office or Region, U. S. Nuclear Regulatory Commission, and mailing address.)

Division of Systems Analysis,
Office of Nuclear Regulatory Research,
U.S. Nuclear Regulatory Commission,
Washington, D.C. 20555-0001.

10. SUPPLEMENTARY NOTES

A. Hsieh, NRC Project Manager

11. ABSTRACT (200 words or less)

This study conducted an assessment of the 3D components in the system codes: TRACE V5 patch 7 and MARS-KS 2.0, against two separate effect tests—GE 3X3 and PSBT bundle experiments. Results from these tests revealed that the 3D components of both codes inadequately predicted the phasic distribution observed in the experiments. These assessment findings underscored the critical significance of crossflow in subchannel-scale analysis. Furthermore, they highlighted the pressing need for improvements in the crossflow models of both codes to accurately predict the appropriate phasic distribution in the bundle. As a proposed enhancement, the study strongly recommended the application of the subchannel mixing model, a prevalent turbulence model widely utilized in state-of-the-art subchannel analysis codes. Notably, the study demonstrated that improving crossflows significantly enhanced the overall code predictability, especially when implementing the subchannel mixing model for the secondary transport of a two-phase mixture.

12. KEY WORDS/DESCRIPTORS (List words or phrases that will assist researchers in locating the report.)	13. AVAILABILITY STATEMENT
GE 3X3, PSBT, TRACE, MARS-KS, crossflow, subchannel mixing	unlimited
	14. SECURITY CLASSIFICATION
	(This Page) unclassified
	(This Report) unclassified
	15. NUMBER OF PAGES
	16. PRICE

NUREG/IA-0551 Assessment of 3D Components in System Codes Against Separate Effect Tests June 2025